Mechanical loading reveals an intrinsic cardiomyocyte stiffness contribution to diastolic dysfunction in murine cardiometabolic disease

Johannes V. Janssens[1,6], Antonia J.A. Raaijmakers[1], Parisa Koutsifeli[3], Kate L. Weeks[1,4], James R. Bell[1,5], Jennifer E. Van Eyk[6], Claire L. Curl[1], Kimberley M. Mellor[2,3,1] and Lea M.D. Delbridge[1]

[1]Department of Anatomy & Physiology, University of Melbourne, Australia

[2]Department of Physiology, University of Auckland, New Zealand

[3]Auckland Bioengineering Institute, University of Auckland, New Zealand

[4]Baker Department of Cardiometabolic Health (Baker), University of Melbourne, Australia

[5]Department of Microbiology, Anatomy, Physiology & Pharmacology, La Trobe University, Australia

[6]Smidt Heart Institute, Cedars-Sinai Medical Center, Los Angeles, USA.

Running Title: *Cardiomyocyte stiffness in diastolic dysfunction*

Key words: *cardiomyocyte; diastolic dysfunction; cardiometabolic disease; stiffness; relaxation; Ca^{2+} myofilament interaction*

A draft version of this manuscript was first published as a preprint: Janssens JV et al (2024). [Mechanical loading reveals an intrinsic cardiomyocyte stiffness contribution to diastolic dysfunction in murine cardiometabolic disease] bioRxiv. 2024.02.21.581448; doi: https://doi.org/10.1101/2024.02.21.581448

Corresponding author:

Prof Lea MD Delbridge

Cardiac Phenomics Laboratory

Department of Anatomy and Physiology,

University of Melbourne, Australia.

lmd@unimelb.edu.au

ABSTRACT

Cardiometabolic syndromes including diabetes and obesity are associated with occurrence of heart failure with diastolic dysfunction. There are no specific treatments for diastolic dysfunction and therapies to manage symptoms have limited efficacy. Understanding of the cardiomyocyte origins of diastolic dysfunction is an important priority to identify new therapeutics. The investigative goal was to experimentally define *in vitro* stiffness (stress/strain) properties of isolated cardiomyocytes derived from rodent hearts exhibiting diastolic dysfunction *in vivo* in response to dietary induction of cardiometabolic disease.

Mice fed a High Fat/Sugar Diet (HFSD vs control) for at least 25 weeks exhibited glucose intolerance, obesity and diastolic dysfunction (echo E/e'). Intact paced cardiomyocytes were functionally investigated in three conditions: non-loaded, loaded and stretched.

Mean stiffness of HFSD cardiomyocytes was 70% higher than control. The E/e' doppler ratio for the origin hearts was elevated by 35%. A significant relationship was identified between *in vitro* cardiomyocyte stiffness and *in vivo* dysfunction severity. With conversion from non-loaded to loaded condition, the decrement in maximal sarcomere lengthening rate was more accentuated in HFSD cardiomyocytes (vs control). With stretch, the Ca^{2+} transient decay time course was prolonged. With transition from 2-4Hz pacing, HFSD cardiomyocyte stiffness was further increased, yet diastolic Ca^{2+} rise was 50% less than control.

Collectively, these findings demonstrate that a component of cardiac diastolic dysfunction in cardiometabolic disease is derived from intrinsic cardiomyocyte mechanical abnormality. Differential responses to load, stretch and pacing suggest that a previously undescribed alteration in myofilament-Ca^{2+} interaction contributes to cardiomyocyte stiffness in cardiometabolic disease.

57 **KEY POINTS**

58

59 • Understanding cardiomyocyte stiffness components is an important priority for identifying new
60 therapeutics for diastolic dysfunction, a key feature of cardiometabolic disease.

61

62 • In this study cardiac function was measured *in vivo* (echocardiography) for mice fed a high-fat/sugar
63 diet (HFSD, ≥25weeks) and performance of intact isolated cardiomyocytes derived from the same
64 hearts was measured during pacing under non-loaded, loaded and stretched conditions *in vitro.*

65

66 • Using a calibrated cardiomyocyte stretch protocol, stiffness (stress/strain) was elevated in HFSD
67 cardiomyocytes *in vitro* and correlated with diastolic dysfunction (E/e') *in vivo*.

68

69 • The HFSD cardiomyocyte Ca^{2+} transient decay was prolonged in response to stretch, and stiffness was
70 accentuated in response to pacing increase while the rise in diastolic Ca^{2+} was attenuated.

71

72 • These findings suggest that stretch-dependent augmentation of the myofilament-Ca^{2+} response during
73 diastole partially underlies elevated cardiomyocyte stiffness and diastolic dysfunction of hearts of
74 animals with cardiometabolic disease.

75

76

77 **INTRODUCTION**

78

79 Increasingly, cardiometabolic syndromes, including diabetes and obesity, are associated with occurrence of
80 heart failure with a diastolic dysfunction patho-phenotype (Sotomi *et al.*, 2021). Diastolic dysfunction is
81 characteristic of heart failure with preserved ejection fraction (HFpEF) which has now overtaken heart
82 failure with reduced ejection fraction (HFrEF) comprising the majority of new heart failure diagnoses
83 (McHugh *et al.*, 2019; Jackson *et al.*, 2022). Diastolic dysfunction is also linked with progression of diabetic
84 cardiomyopathy (Patil *et al.*, 2011; Redfield, 2016). With both HFpEF and diabetic heart disease, early
85 development of diastolic dysfunction can be detected even when other phenotypic features/comorbidities
86 are heterogeneous (i.e. hypertrophy, dilation, natriuretic factor elevation, hypertension) (Kittleson *et al.*,
87 2023). Common clinical features of cardiometabolic syndromes, including obesity and insulin resistance, are
88 independent risk factors for diastolic dysfunction as a prelude to heart failure (Rozenbaum *et al.*, 2019;
89 Kamon *et al.*, 2020). Cardiometabolic syndromes can involve the 'silent' presence and progression of
90 diastolic dysfunction for an extended period. Symptoms can be subclinical and/or detectable only in
91 challenge conditions (i.e. as reduced diastolic reserve in exercise) or when exacerbated by co-morbidity
92 (Leung *et al.*, 2015; Lam *et al.*, 2019). Diagnosis of heart failure with diastolic dysfunction is independently
93 associated with higher incidence of adverse clinical events (Sotomi *et al.*, 2021). Notably, there is currently
94 no specific treatment for diastolic dysfunction and/or HFpEF, and therapies to manage symptoms have
95 limited efficacy (Delbridge *et al.*, 2022).

96

97 In diastolic dysfunction, the relaxation and filling phases of the cardiac cycle are impaired. The condition is
98 generally described qualitatively as an increase in left ventricular wall 'stiffness' (or by a decrease in
99 compliance, the inverse of stiffness) (Daniels *et al.*, 2022; Janssens *et al.*, 2024). Clinically and
100 experimentally, reduced compliance can be measured invasively as an elevation in left ventricular filling
101 pressure or an increase in the gradient of the diastolic pressure-volume relationship. Non-invasively, on
102 doppler echocardiogram, an increase in the E/e' ratio [early (E) mitral valve blood flow rate to early mitral
103 annulus tissue motion (e')] is an index used to identify diastolic abnormality (Lo & Thomas, 2010).

104

105 Myocardial stiffness is commonly considered to reflect myocardial extracellular matrix abnormalities linked
106 with increased tissue fibrosis. While a component of reduced compliance likely reflects fibrotic infiltration,
107 diastolic dysfunction can be identified in settings where there is no evidence of increased interstitial fibrosis
108 burden (Curl *et al.*, 2018). There is growing appreciation that alterations of myocardial compliance in
109 diastolic dysfunction disease states represents underlying intrinsic cardiomyocyte stiffness pathology which
110 contributes to impaired relaxation and filling (Zhou & Pu, 2016; Villalobos Lizardi *et al.*, 2022).
111 Understanding the cardiomyocyte origin of diastolic dysfunction is an important priority to identify new

112 molecular targets and to support the development of new diagnostics and therapeutics to reduce
113 morbidity and mortality in cardiometabolic disease states.
114
115 Cardiomyocyte origins of diastolic dysfunction potentially comprise structural and operational components.
116 Evidence of molecular changes in sarcomeric and cytoskeletal elements is extensive (Villalobos Lizardi *et al.*,
117 2022; Loescher *et al.*, 2023; Janssens *et al.*, 2024). Operationally, the cardiac cycle of contraction and
118 relaxation is driven by the cyclic flux of cardiomyocyte activator Ca^{2+} to initiate contraction (myocyte
119 sarcomere shortening) and to allow relaxation (myocyte sarcomere lengthening). The relationship between
120 cytosolic Ca^{2+} levels and myofilament activation is dynamic and depends on several external factors some
121 of which include stretch and pacing (Fabiato & Fabiato, 1978; Varian & Janssen, 2007).
122
123 Conventionally, the steady-state force-Ca^{2+} analysis (typically performed in permeabilised, quiescent
124 preparations) is used to summarise the myofilament-Ca^{2+} response and is the product of many complex
125 myofilament protein interactions. Less work has been done to investigate the dynamic changes in the
126 myofilament-Ca^{2+} relationship in paced intact cardiomyocytes, especially in disease contexts. In diastolic
127 dysfunction, specifically in HFpEF animal models, evidence is accruing that Ca^{2+} deficit and impaired non-
128 loaded shortening *are not* phenotypic (Kilfoil *et al.*, 2020). Indeed cardiomyocyte myofilament hyper-
129 activation and elevated Ca^{2+} levels have been reported (Curl *et al.*, 2018; Louch, 2020; Saad *et al.*, 2023). As
130 we have recently proposed, the role for elevated diastolic Ca^{2+} levels and augmented myofilament-Ca^{2+}
131 response comprising a cross-bridge derived component of cardiomyocyte diastolic stiffness is increasingly
132 plausible (Janssens *et al.*, 2024). This experimental enquiry focusses on intact cardiomyocyte mechanical
133 and Ca^{2+} performance in response to load, stretch and modulated pacing conditions.
134
135 While the term 'stiffness' is used as a general descriptor of impaired compliance in a cardiovascular setting,
136 it is more formally specified quantitatively in physical science disciplines (Mirsky, 1976). Stiffness is defined
137 as the force per cross-sectional area (stress) developed with application of a normalized stretch or
138 deformation (strain) to a material. The ratio of stress/strain defines stiffness of the material and is known
139 as 'Young's Modulus'. In the cardiac setting, a stretch or deformation state is commonly described as
140 'loading' – for example 'pre-load' (diastolic stretch) and 'after-load' (resistance to shortening). Depending
141 on the experimental design, stiffness behaviour of myocardial tissues, active cardiomyocytes and/or
142 myocyte sub cellular cytoskeleton and sarcomere structures all potentially contribute to *in vivo* functional
143 stiffness. Little is known about how stiffness measured at different structural levels may determine function
144 *in vivo* and how stiffness elements are quantitatively changed in pathophysiology – in particular in acquired
145 disease conditions. Thus, the goal of this investigation was to experimentally characterize *in vitro* stiffness
146 properties (stress/strain) of cardiomyocytes derived from hearts of animals exhibiting diastolic dysfunction
147 *in vivo* in the setting of dietary induction of cardiometabolic disease.

148 **METHODS & MATERIALS**

149

150 **Animal model of cardiometabolic disease**

151 As a pre-clinical cardiometabolic disease model, the high fat/sugar diet (HFSD) fed rodent recapitulates a
152 common and growing human disease phenotype (obesity, insulin resistance, glucose intolerance) and has
153 been established as a diastolic dysfunction model (Heather *et al.*, 2022). Cardiometabolic disease was
154 induced in male C57Bl/6J mice by a high fat/sugar dietary intervention commencing at 8-9 weeks of age.
155 Animals were randomized to experimental treatment groups and were group housed (> 4 animals per cage)
156 in a temperature-controlled environment 21-23°C with 12 hour light/dark cycles. After 1 week transitional
157 feeding period (alternating feed periods), animals were fed a HFSD (43% kcal from fat, 200g/kg sucrose,
158 SF04-001, Specialty Feeds) or control reference diet (CTRL: 16% kcal from fat, 100g/kg sucrose, AIN93G,
159 Specialty Feeds) for at least 25 weeks. All animal experiments were approved by the University of
160 Melbourne (School of Biomedical Sciences) Animal Ethics Committee and complied with the guidelines and
161 regulations of the Code of Practice for the Care and Use of Animals for Scientific Purposes (National Health
162 and Medical Research Council Australia).

163

164 **Glucose tolerance testing**

165 At 23-25 weeks of feeding, glucose tolerance testing was performed in mice following 6 hours fasting as
166 previously described (Chandramouli *et al.*, 2018). Baseline blood glucose levels were measured using an
167 Accu-Chek glucometer with a blood sample obtained from a needle prick to the tail vein. Glucose (1.5 g/kg
168 body weight) was injected i.p. and blood glucose was measured at 5, 15, 30, 60 and 90 minutes after the
169 glucose injection.

170

171 **Transthoracic echocardiography**

172 At 25-26 weeks of feeding, cardiac structure, systolic and diastolic function were evaluated by transthoracic
173 2-dimensional B- and M-mode and blood flow and tissue doppler echocardiography (GE Vivid 9; 15mHz i13L
174 linear array transducer) as described previously (Chandramouli *et al.*, 2018; Curl *et al.*, 2018). Briefly, mice
175 were lightly anesthetised with Isoflurane (1.5%; Baxter healthcare, Australia). Parasternal short axis view
176 was used to measure morphological and systolic parameters (interventricular septum IVS, left ventricular
177 posterior wall LVPW, left ventricular internal dimension LVID, fractional shortening FS, ejection fraction EF,
178 heart rate HR). Pulse wave Doppler and tissue Doppler scans were acquired from the apical 4 chamber view
179 to assess LV diastolic function parameters: velocity of early (E) and late (A) mitral inflow and early (e') and
180 late (a') diastolic velocity of mitral annulus. From these compound indices of diastolic function E/e', E/A and
181 e'/a' were calculated. In addition, the slope of the E wave was used to calculate mitral valve deceleration
182 time. Three consecutive cardiac cycles were sampled for each measurement.

183

184 **Cardiomyocyte preparation, structural and functional assessment**

185 A series of protocols were implemented to phenotype cardiomyocyte and sarcomere morphology, and
186 assess functional status in different contraction configurations and challenge settings.

187

188 ***Cardiomyocyte isolation, morphology & microfluorimetry.*** HFSD and CTRL left ventricular cardiomyocytes
189 were enzymatically isolated using methods previously described (Howlett *et al.*, 2006; Mellor *et al.*, 2011)
190 at 30-32 weeks feeding. Briefly, the heart was excised, cannulated via the aorta, and subjected to
191 retrograde perfusion on a Langendorff apparatus with an oxygenated Ca^{2+} free buffer at 37°C for 10
192 minutes. The buffer was composed of (in mM): 130 NaCl, 5 KCl, 0.33 NaH_2PO_4; 1 $MgCl_2$, 25 HEPES; 20
193 Glucose; 3 Na Pyruvate; 1 Na Lactate. The Ca^{2+} free buffer was then supplemented with 0.66mg/mL
194 collagenase (Worthington; Type II), 0.033mg/mL trypsin and 0.05mM $CaCl_2$ and perfusion continued for a
195 further 10 minutes. The heart was removed from the Langendorff apparatus, and the left ventricle was
196 segmented into small pieces in a high potassium solution composed of (in mM): 30 KCl, 90 KOH, 30 KH_2PO_4,
197 3 $MgSO_4$, 50 glutamic acid, 20 taurine, 0.5 EGTA, 10 glucose, and 10 HEPES. Single left ventricular
198 cardiomyocytes were isolated via gentle trituration. Viable cardiomyocytes were resuspended in HEPES-
199 Krebs buffer (in mM); 146.2 NaCl, 4.69 KCl, 0.35 $NaH_2PO_4H_2O$, 1.05 $MgSO_47H_2O$, 10 HEPES, 11 glucose
200 containing 1.8mM Ca^{2+} and were stored on a rocking platform at room temperature. From each heart cell
201 dimensions were collected from at least 50 rod shaped cardiomyocytes using an inverted light microscope
202 (Nikon) and calibrated eye piece as previously described (Curl *et al.*, 2018). Cardiomyocyte volume was
203 calculated by inserting experimentally determined myocyte length and width values into the formula:
204 volume =length x width x depth x multiplier 0.54 (elliptical area of the rectangle defined by width & length,
205 (Satoh *et al.*, 1996)). Cardiomyocyte width: depth ratio was assumed to be 1.44 (Natali *et al.*, 2001).
206 Cardiomyocyte cross-sectional area (CSA) could be calculated from measured width scaled for
207 2-dimensional geometry (CSA = W [W/1.44] x 0.54 μm^2). An aliquot of isolated cardiomyocyte suspension
208 was pipetted into a cell chamber mounted on the stage of an inverted fluorescence microscope (Motic
209 AE31) and superfused with HEPES-Krebs solution with 2mM Ca^{2+}, 37°C at a flow rate of 2mL/min.
210 Cardiomyocyte sarcomere length and Ca^{2+} transients were simultaneously recorded during isotonic
211 contractions. Myocyte force development was evaluated in the same cells with transducer attachment,
212 using four protocols described below.

213

214 ***Characterizing cardiomyocyte diastolic function: non-loaded shortening measurements (isotonic), loaded***
215 ***force measurements (auxotonic), stretch responses and pacing challenge.*** Cardiomyocyte performance
216 was evaluated in several paced conditions: designated 'non-loaded' (isotonic), 'loaded' (auxotonic after-
217 loaded), and 'stretched'(auxotonic pre-loaded). The non-loaded state refers to the absence of externally
218 applied load (noting that sarcomeric and cytoskeletal structures do constitute an underlying internal load).

219

220 Firstly, cardiomyocyte non-loaded (isotonic) sarcomere contractions (IonOptix SarcLen, Fast Fourier
221 Transform, FFT) and Ca^{2+} transients (Fura2-AM, 5µM microfluorimetry F340:380nm ratio) were
222 simultaneously measured at 2Hz, using a microscope diaphragm to define a rectangular intra-myocyte
223 region of interest as depicted **Fig. S1**. During contraction cycles, cardiomyocyte sarcomere length was
224 monitored within an intracellular region of interest defined by an adjustable diaphragm mounted in the
225 microscope optical tube (**Fig S1A**).
226
227 Secondly, to obtain loaded (auxotonic) contraction data, each cardiomyocyte was attached to a pair of glass
228 fibres coated with a bio-adhesive (MyoTak, IonOptix, USA). Attachment sites were positioned to be outside
229 the sarcomere tracking region, closer to myocyte longitudinal ends. One glass fibre was connected to a
230 force transducer (fibre stiffness 20N/m, IonOptix, USA), and the other to a piezo-motor (Nano-drive, Mad
231 City Labs Inc. WI, USA) to adjust cardiomyocyte length. With successful attachments, cardiomyocytes were
232 lifted from the coverslip using motorised micromanipulators (MC1000E, Siskiyou Corporation, USA)
233 attached to both the force transducer and the piezo-motor. Baseline loaded contractions at 2Hz were
234 recorded. Sarcomere length changes were measured using FFT as described above. In addition, with glass
235 fibre attachment, tracking of mean sarcomere shortening within a myocyte segment delineated by the
236 glass fibre edge positions could be performed in parallel.
237
238 Thirdly, force was recorded during a standardized stretch protocol of loaded cardiomyocytes to measure
239 the effect of increasing diastolic cardiomyocyte/sarcomere basal length during pacing. A stress-length
240 relation was constructed for each myocyte (where stress = force/cross-sectional area). Prior to the
241 commencement of the myocyte stretch measurements a protocol to calibrate the stretch step was
242 implemented. Four consecutive 0.5V input signals were delivered to the piezo-motor to determine a
243 calibration constant to define the percentage cell stretch for a given voltage. For each myocyte a
244 *Calibration Constant* was calculated as: *myocyte segment length change per peizomotor mV / sarcomere*
245 *count in segment* [where *myocyte sarcomere count = myocyte segment length (µm) / average diastolic*
246 *sarcomere length (µm)*]. To track the glass fibre position a real-time contrast detection algorithm (IonOptix -
247 EdgeLength) was focused on the internal edge of each of the glass fibres (**Fig. S1**) (Peyronnet *et al.*, 2017).
248 This enabled reproducible and comparable stretch steps to be applied to different cardiomyocyte
249 preparations (**Fig. S1B-C**). Prior to the 'stress-length' protocol, a cell-specific calibration constant was
250 applied to yield a standardised stretch for each cardiomyocyte evaluated. The stress-length protocol
251 involved progressive stretch steps totaling an approximate 30% cell stretch (**Fig. S1B-C**).
252
253 Lastly, the pacing was increased to 4Hz, a rate adaptation period allowed (2mins) and the stress-length
254 protocol was repeated. Sarcomere length, force development and intracellular Ca^{2+} transients were
255 simultaneously measured. In summary, the following parameters were measured: diastolic stress

256 (mN/mm^2), diastolic stress-length relation [(mN/mm^2) / (%$^-$ length change)], diastolic stress-sarcomere
257 length relations ((mN/mm^2) / µm), sarcomere shortening (% diastolic SL), maximum sarcomere shortening
258 and lengthening velocity (µm/s). In addition, Ca^{2+} parameters were measured: diastolic Ca^{2+}, systolic Ca^{2+}
259 and time constant of decay of the Ca^{2+} transient (tau).
260
261 **Statistical analyses**
262 Data are presented as mean ± SEM and statistical analysis was performed using GraphPad Prism V9.5.1.
263 Cardiomyocyte stress-length and stress-SL relations were modelled with simple linear regression. For
264 comparison between two groups an unpaired student t-test was used. For assessment between two groups
265 at multiple points a one-way ANOVA with Bonferroni multiple comparisons post-hoc test was used. Two-
266 way ANOVA with Šídák's multiple comparisons post-hoc test was used for the evaluation of data groups
267 with two independent variables. Pearson Correlation analyses were used to assess statistical significance of
268 fitted linear regression lines. A p-value of <0.05 was considered statistically significant. Analyses were
269 performed using a blinded protocol.
270

271 **RESULTS**

272

273 **Systemic indicators of cardiometabolic disease and *in vivo* diastolic function in HFSD mice**

274 High fat/sugar diet-fed mice exhibited obesity and glucose intolerance. Relative to CTRL, the body weight of
275 HFSD mice was significantly elevated within 5 weeks of dietary intervention increasing over the study
276 duration by 50% relative to CTRL (**Fig. 1A**, CTRL: 29.5±0.5 vs. HFSD: 45.7±1.2g). After 23-24 weeks diet
277 treatment, glucose tolerance testing of a subset of the HFSD cohort was performed. Glucose intolerance in
278 response to intraperitoneal glucose administration was evidenced by increased area under the curve,
279 consistent with literature reporting insulin resistance in mice fed a similar diet (**Fig. 1B**).

280

281 After confirming these key cardiometabolic disease characteristics in the HFSD mice, echocardiographic
282 functional evaluation was undertaken. Focusing on diastolic function evaluation (**Fig. 1C-G**), there was
283 increased early mitral inflow (**Fig. 1D,** E wave, CTRL: 476.8±19.9, HFSD: 554.6±16.8 mm/s) and reduced
284 velocity of wall motion (**Fig. 1E,** e' wave, CTRL: 28.5±1.3, HFSD: 25.2±0.9 mm/s) in HFSD myocardium.
285 Deceleration time of mitral inflow was shortened (**Fig. 1F,** CTRL: 31.5±2.2, HFSD: 19.7±1.5 ms) and E/e' ratio
286 increased (**Fig. 1G,** CTRL: 16.7±1.0, HFSD: 22.3±1.5), all observations consistent with reduced tissue
287 compliance and diastolic dysfunction. No differences in systolic performance parameters were observed
288 (**Table S1**), confirming the primary *in vivo* phenotype of diastolic dysfunction. The next step was to evaluate
289 the cardiomyocyte involvement in dysfunction.

290

291 **Non-loaded sarcomere and Ca^{2+} dynamics in CTRL and HFSD cardiomyocytes**

292 Single isolated cardiomyocytes were prepared from hearts of a subset of mice which underwent
293 echocardiographic analyses. For intact, non-loaded cardiomyocytes sarcomere shortening and lengthening
294 cycles were similar for CTRL and HFSD groups (**Fig. 2A**). Diastolic sarcomere length (SL) (**Fig. 2B**, CTRL:
295 1.71±0.01, HFSD: 1.72±0.01 µm) and extent of sarcomere shortening (**Fig. 2C**, CTRL: 3.79±0.33, HFSD:
296 3.94±0.40 % diastolic SL) were not different between groups. Examination of sarcomere contraction
297 kinetics (**Fig. 2D** exemplar trace) showed that the maximum rate of lengthening (**Fig. 2E**, CTRL: 1.08±0.14,
298 HFSD: 1.29±0.18 µm/s) and shortening (**Fig. 2F**, CTRL: -2.32±0.21, HFSD: -2.57±0.28 µm/s) did not differ
299 between CTRL and HFSD groups. Collectively these findings indicate that in the non-loaded setting no
300 differences in CTRL and HFSD cardiomyocyte systolic and diastolic non-loaded performance were detected,
301 a finding consistent with other studies investigating non-loaded cardiomyocyte performance in diet-
302 induced cardiometabolic disease including our previous studies in fructose-fed mice (Mellor *et al.*, 2012;
303 Llano-Diez *et al.*, 2016; West *et al.*, 2019; Wang *et al.*, 2020).

304

305 Next, Ca^{2+} parameters were compared with cardiomyocyte sarcomere lengthening performance during
306 relaxation and diastole (**Fig. 2G**, exemplar traces). No significant difference was evident between dietary

307 treatment groups in the systolic Ca^{2+} (**Fig. 2H**, CTRL: 1.098±0.028, HFSD: 1.171±0.032 $F_{340:380}$), diastolic Ca^{2+}
308 (**Fig. 2I**, CTRL: 0.749±0.016, HFSD: 0.761±0.017 $F_{340:380}$) or time constant (tau) of Ca^{2+} transient decay (**Fig.2J**,
309 CTRL: 0.160±0.011, HFSD: 0.137±0.009 sec). Thus, the significant diastolic dysfunction measured *in vivo* for
310 the HFSD group was not observed in a non-loaded *in vitro* setting. To reconcile the impaired
311 echocardiographic heart performance with absence of dysfunction in non-loaded contracting single
312 cardiomyocytes, the next strategy was to assess single cardiomyocyte response to loading. A common
313 feature of cardiometabolic disease is elevation in after-load – i.e. elevated systemic resistance potentially
314 impeding myocardial pump function. To simulate this *in vitro*, mechanically loaded cardiomyocyte
315 performance was examined.
316
317 **Loaded cardiomyocyte sarcomere shortening and lengthening**
318 Immediately after non-loaded cardiomyocyte recordings, glass fibres were attached to cardiomyocyte
319 longitudinally separated positions to permit auxotonic, loaded contraction measurements. For cells
320 successfully attached, the mean difference in sarcomere length measured pre- and post-conversion to
321 loaded mode was <0.02% diastolic length, indicating non-loaded and loaded sarcomere initial lengths were
322 well matched. For attached cardiomyocytes, a comparison of sarcomere shortening behavior in the loaded
323 state could be made (using FFT) to directly match with data obtained non-loaded state.
324
325 With loading, for all myocytes (both treatment groups), extent of sarcomere shortening was reduced and
326 shortening and lengthening kinetics slowed when compared with non-loaded performance (**Fig. 3A**). Mean
327 data showed that in response to loading, sarcomere shortening was reduced by ~34% (**Fig. 3B**, non-loaded:
328 0.075±0.008, loaded: 0.050±0.006 µm). Maximum rate of shortening was decreased by 58% (non-loaded: -
329 2.85±0.28, loaded: -1.20±0.18 µm/s; not shown), and maximum rate of lengthening by 66% (**Fig. 3C**, non-
330 loaded: 1.46±0.21, loaded: 0.52±0.10 µm/s). The magnitude of the change in extent of shortening and
331 maximum rate of lengthening with loading were positively correlated (**Fig. 3D**) suggesting the possibility of
332 common underlying mechanisms.
333
334 To assess cardiomyocyte rate kinetics in non-loaded and loaded cardiomyocytes independent of shortening
335 extent, the maximum rates of lengthening and shortening were normalised by shortening amplitude to
336 derive 'deformation rate' - i.e. rate of length change, relative to extent of shortening (units µm x sec-1)/µm
337 = 1/sec). The effect of loading on deformation rate was accentuated in HFSD group (significant ANOVA diet
338 x load interaction effect, **Fig. 3E**). A selective HFSD effect was revealed in the differential between matched
339 'loaded' and 'non-loaded' lengthening cardiomyocytes. The decrement in deformation rate (lengthening)
340 for CTRL and HFSD is shown in **Fig. 3F**, and is accentuated in HFSD in response to loading (CTRL: 7.38±1.15,
341 HFSD: 12.70±2.23 1/s). Treatment differences in deformation rate were not evident during the shortening
342 phase (data not shown)**.** These findings indicated an accentuated influence of load, specific to the

343 lengthening (i.e. diastolic) phase in HFSD cardiomyocytes and could reflect impaired subcellular relaxation
344 processes specific to the HFSD myocardium. Based on these data identifying different CTRL and HFSD origin
345 cardiomyocyte responses in loaded state, we next investigated the effect of stretch applied to
346 cardiomyocytes to simulate *in vivo* 'pre-load' conditions.
347
348 **Cardiomyocyte force development: measuring strain & stress during progressive cardiomyocyte stretch**
349 A hallmark of diastolic dysfunction is an elevated diastolic pressure-volume relationship which describes
350 the increased resistance of the myocardial wall to chamber filling (Aurigemma *et al.*, 2006). We sought to
351 design a single cardiomyocyte version of this relationship (Fowler *et al.*, 2015), by applying standardized
352 stretch steps to cardiomyocytes, defining the steps as a % of non-stretched state (i.e. 'strain'). Diastolic
353 force was measured simultaneously during length stretch steps. The force measured at every strain
354 increment was normalized by cross sectional area (CSA) to produce a measure of 'stress' (i.e. force/CSA,
355 mN/mm^2). Thus a sarcomere 'stress/strain' relation (i.e. force-length) was constructed for each myocyte.
356 The protocols employed to generate stress-strain are depicted in **Fig. S1** and described in detail in the
357 Methods. **Fig. S1** shows the stretch standardization approach used to enable reproducible application of
358 strain (converting voltage signals to linear displacement) as a % length change (via individual myocyte
359 calibration constant calculation) to allow comparisons between different cardiomyocytes. The size of each
360 step change in length on sarcomere length was measured (FFT) and confirmed by tracking the intra-
361 cardiomyocyte segment between the glass fibres (**Fig. S1**). In some cases a direct sarcomere FFT measure
362 was not microscopically resolvable due to myocyte contraction responses which partially positioned some
363 area of the myocyte outside the optimal focal plane. In these situations it was always possible to calculate
364 segment length change. For the example shown, stretch steps were determined to be 2.75µm, and
365 converted to % sarcomere length (i.e. strain) using sarcomere count within intracellular region of interest
366 area (**Fig. S1C**). A comparison of the variability of cell stretches performed using a uniform (pre-set) stretch
367 constant and the individually derived stretch calibration constant demonstrates that reproducibility is
368 optimized with usage of the individual stretch calibration constant data (**Fig. S1D**). Force, sarcomere length
369 and % stretch were measured simultaneously (**Fig. S1**).
370
371 **Quantifying diastolic stiffness in CTRL vs HFSD cardiomyocytes using strain normalization methods**
372 Superimposed exemplar stress recordings are shown in **Fig. 4A** for CTRL and HFSD cardiomyocytes,
373 captured during a series of progressive stretches during a 100 sec period. The dashed (broken) lines are
374 aligned with the diastolic stress step increments for each of the 2 myocytes (using the data points collected
375 prior to the transition to a new step) throughout the series of progressive stretches. A robust increase in
376 systolic force with stretch is also evident, indicative of length-dependent activation, the cardiomyocyte
377 basis for the Frank-Starling mechanism.
378

379 In this experimental setting, stiffness could be visualized as the gradient of the linear plot derived from the
380 cardiomyocyte diastolic stress-length relation. Our stretch protocol methodology provided two approaches
381 for stiffness calculation (as per Methods). A first approach used FFT measurement of sarcomere length to
382 track cardiomyocyte stretch and was plotted according to the standardized stretch steps (in units µm). An
383 alternative approach used percent length change calculated as the length of the cardiomyocyte segment
384 between the glass attachment fibres divided by the initial distance between the fibres prior to stretch (in
385 units % initial length).
386
387 Applying the first approach, a linear regression was performed to fit the data from which a slope value
388 could be derived. **Fig. 4B** depicts the average diastolic and systolic stress-sarcomere length relations for
389 CTRL cardiomyocytes only. To determine cardiomyocyte diastolic stiffness using FFT-computed sarcomere
390 length values, the gradient of the mean slope of the diastolic stress sarcomere-length relation for each
391 treatment group was calculated, using mean sarcomere length change (µm) as the denominator. This
392 gradient was significantly higher in HFSD myocytes compared to CTRL (**Fig. 4C**). The individual slope
393 gradients were used to calculate the mean diastolic stress / strain gradient (**Fig. 4D,** CTRL: 2.40±0.72, HFSD:
394 5.50±1.51 (mN/mm^2) / µm), p = 0.067) where there was a trend for a 2.3 fold increase in stiffness of HFSD
395 cardiomyocytes. The statistical power of this analysis was limited due to the difficulty in achieving
396 resolvable diastolic sarcomere lengths by FFT for all myocytes.
397
398 Applying the second approach, it was possible to construct stress-segment length (%) relations for all
399 myocytes from which stress data could be obtained. In **Fig. 4E**, the stress-segment length data for HFSD and
400 CTRL are shown, with a robustly significant difference detected in mean gradient values. In **Fig. 4F** the
401 diastolic stress/strain values calculated for the myocytes from the two treatment groups using this segment
402 approach are directly compared. The HFSD cardiomyocyte stiffness index derived using this approach was
403 increased by 70% compared with CTRL (**Fig. 4F**, CTRL: 0.0075±0.0016, HFSD: 0.0128±0.0016 ((mN/mm^2) / %
404 length).
405
406 To examine the relationship between intrinsic *in vitro* cardiomyocyte stiffness and *in vivo* diastolic
407 dysfunction, diastolic stiffness (slope of the diastolic stress segment-length relation) averaged per animal
408 was plotted against the E/e' index of diastolic dysfunction. There was a significant correlation between
409 cardiomyocyte stiffness and E/e' in HFSD and no evidence of a relationship for the CTRL group (**Fig.4G** CTRL:
410 p=ns, HFSD: p=0.0096, r^2=0.9213). These data support the interpretation that intrinsic cardiomyocyte
411 stiffness represents a definable and inherent component of diastolic dysfunction occurring *in vivo* in
412 cardiometabolic disease.
413
414

415 **Load dependence of Ca^{2+} transient decay in CTRL and HFSD cardiomyocytes**

416 To further understand the cardiomyocyte functional elements comprising increased intrinsic stiffness in
417 cardiopathology, the relationship between Ca^{2+} transient features and myofilament deactivation in
418 response to progressive stretch was evaluated. In the intact cardiomyocyte model these electro-mechanical
419 coupling processes are functional for interrogation (in contrast to the disrupted cytosolic environment
420 which characterizes permeabilized myocyte preparations). The Ca^{2+} transient decay features were
421 compared for non-loaded and loaded basal states and also in response to progressive stretch.
422
423 In CTRL cardiomyocytes there was no difference in the time constant of Ca^{2+} transient decay (tau, 1/e)
424 between loaded and stretched state (20% increase in length, **Fig. 5A.** loaded 1.12±0.14; stretched
425 1.09±0.10 fold change vs non-loaded reference 1.00±0.12). In HFSD cardiomyocytes the time constant of
426 Ca^{2+} transient decay was increased in stretched cardiomyocytes relative to non-loaded (**Fig. 5A**. non-
427 loaded, 1.00±0.12; loaded: 1.22±0.15; stretched 1.42±0.19 fold change). A trend for an interaction effect
428 (p=0.055) between diet and load was observed, suggesting potential for a differential Ca^{2+} transient
429 response to load between CTRL and HFSD cardiomyocytes. The effects can be visualized in **Fig. 5B-C** where
430 the mono-exponential decay of exemplar Ca^{2+} transients is depicted. The shallower decay of the Ca^{2+}
431 transient in the stretched state (**Fig 5C**, HFSD) was apparent whereas the loaded and non-loaded decay
432 traces were virtually overlayed for CTRL cardiomyocytes (**Fig. 5B**). These data suggest that stretch may
433 enhance a mechanism by which the myofilaments bind Ca^{2+} for a prolonged duration during relaxation thus
434 reducing Ca^{2+} availability for extrusion from the cytosol.
435
436 **Pacing-induced $[Ca^{2+}]_i$ increase to examine potential for a cross-bridge derived stiffness mechanism**

437 A further mechanistic study to probe the potential relationship between Ca^{2+} and stiffness involved
438 perturbation of cytosolic Ca^{2+} cycling time. Elevating stimulation frequency is a recognized physiologic
439 strategy to increase diastolic Ca^{2+} levels and to apply increased cardiomyocyte workload. In response to
440 frequency elevation (2Hz to 4Hz) cardiomyocyte diastolic Ca^{2+} levels increased in both CTRL and HFSD (**Fig.**
441 **6A & B**) groups consistent with previous studies (Varian & Janssen, 2007; Eisner *et al.*, 2020). In the HFSD
442 cardiomyocytes this effect was markedly diminished and about half the mean magnitude of the Ca^{2+} shift
443 observed for CTRL myocytes (**Fig. 6B.** CTRL 2Hz: 0.662±0.017, CTRL 4Hz: 0.775±0.028, HFSD 2Hz:
444 0.688±0.035, HFSD 4Hz: 0.741±0.045, $F_{340:380}$, 2-way ANOVA significant interaction effect, **Fig. 6C**. CTRL
445 0.111±0.017; HFSD 0.054±0.017, $F_{340:380}$). Frequency elevation was associated with a reduction in diastolic
446 sarcomere length in both CTRL (3%) and HFSD (5%) loaded cardiomyocytes (**Fig. 6D**. CTRL 2Hz: 1.69±0.01,
447 CTRL 4Hz:1.64±0.020, HFSD 2Hz: 1.69±0.014, HFSD 4Hz: 1.61±0.023 µm). The combination of normal
448 diastolic sarcomere length reduction, concomitant with suppressed diastolic Ca^{2+} increase in HFSD
449 cardiomyocytes, may indicate elevated diastolic responsiveness to Ca^{2+} in the HFSD cardiomyocyte.
450

While frequency elevation did not change the stress/strain relation in CTRL cardiomyocytes, a significant increase in the stress/strain gradient was observed with increased frequency in HFSD cardiomyocytes (**Fig. 6E&F**. CTRL 2Hz: 0.0060±0.0020, CTRL 4Hz:0.0068±0.0024; HFSD 2Hz: 0.0121±0.017, HFSD 4Hz: 0.0136±0.0017 (mN/mm^2) / % length). This may indicate a larger population of cross-bridges contributing to diastolic stiffness at heightened workloads in HFSD cardiomyocytes although other potential non-cross-bridge sources cannot be excluded. Since Ca^{2+} shift in response to increased pacing is modest (relative to CTRL), increase in stiffness cannot be attributed to rise in Ca^{2+} levels *per se.* Shift in the myofilament-Ca^{2+} response during diastole is a potential alternate explanation.

461 **DISCUSSION**

462

463 Here we provide the first quantitative analysis of intact cardiomyocyte stiffness and performance deficits
464 associated with acquired cardiometabolic disease. We demonstrate that a component of cardiac diastolic
465 dysfunction in cardiometabolic disease derives from intrinsic cardiomyocyte mechanical abnormality.

466

467 The concept of myocardial stiffness is a frequently invoked qualitative descriptor of the pathophysiologic
468 phenotype characterizing diastolic dysfunction. Clinically and experimentally the echocardiography
469 parameter E/e' is used as an index of myocardial stiffness in disease diagnosis. E/e' is a compound measure
470 of cellular and extracellular matrix stiffness contributors. Despite consistent *in vivo* findings, an
471 understanding of the cardiomyocyte-specific contribution to tissue stiffness has been difficult to identify.
472 Using a series of intact single cell recording maneuvers, we have established that the stiffness
473 characteristics of individual isolated cardiomyocytes from normal and dysfunctional hearts can be defined,
474 normalized and compared. Further, a significant relationship was identified between the mean stiffness of
475 single cardiomyocytes and the extent of the origin heart diastolic dysfunction (i.e. E/e' vs Young's Modulus).

476

477 To recapitulate, cardiometabolic disease induced by dietary intervention in mice was characterized by
478 marked body weight elevation (50%, 'obesity') and glucose intolerance. *In vivo* echocardiography
479 diagnosed significant diastolic dysfunction with a 35% elevation of the E/e' in HFSD animals (**Fig. 1**) in
480 absence of systolic functional deficit (**Table S1**). In paced non-loaded conditions, the sarcomere contraction
481 cycles & Ca^{2+} transients (fura-2) were similar in CTRL and HFSD cardiomyocytes (**Fig. 2**). When the same
482 cardiomyocytes were loaded, the shortening extent and maximal lengthening rate (**Fig. 3A-C**) were reduced
483 for both diet conditions. In HFSD cardiomyocytes the reduction in deformation rate during lengthening (but
484 not shortening) was accentuated (**Fig. 3E-F**), indicating a selective negative impact of loading on relaxation
485 of the HFSD-derived cardiomyocytes. In HFSD cardiomyocytes there was a larger increase in diastolic force
486 per cross-sectional area (stress: mN/um^2) in response to standardized step increases in length (strain: %
487 initial length[um]) (**Fig. 4A-F**). From these data a 'stress/strain' parameter was determined, defining
488 diastolic stiffness for each myocyte i.e. 'Youngs Modulus' ([$mN/\mu m^2$]/[% initial length[µm]). Mean stiffness
489 was 70% higher in cardiomyocytes of HFSD animals (**Fig. 4F**). Thus the increase in cardiomyocyte stiffness
490 index was approximately double the elevation of the *in vivo* E/e' dysfunction index. Using matched *in vivo*
491 and *in vitro* data, a significant correlation was found between diastolic dysfunction (E/e') and mean
492 cardiomyocyte stiffness value for HFSD-diet animals, while there was no relationship between these
493 parameters in the myocytes of CTRL-diet fed group (**Fig. 4G**). To evaluate possible influence of mechanical
494 state on the Ca^{2+} transient, the mean transient decline parameters (tau) from non-loaded, loaded and
495 stretched cardiomyocytes were compared. In HFSD cardiomyocytes the time constant of Ca^{2+} transient
496 decay was increased in stretched cardiomyocytes relative to non-loaded, a feature not observed in CTRL

497 cardiomyocytes (**Fig. 5**). Finally, in response to an *in vitro* pacing increase HFSD cardiomyocytes exhibited
498 accentuated diastolic stiffness even with a smaller increase in diastolic Ca^{2+} level (**Fig. 6**). Collectively, these
499 findings suggest a previously undescribed alteration in Ca^{2+}-myofilament interactions indicative of a cross-
500 bridge component to cardiomyocyte stiffness in cardiometabolic disease.
501
502 **Dietary model of acquired metabolic syndrome and cardiac diastolic disease**
503 High fat/sugar diet feeding (i.e. 'western diet') has previously been shown experimentally to induce
504 diastolic dysfunction in rodents with prolongation of isovolumic relaxation time (Pulinilkunnil *et al.*, 2014;
505 Dia *et al.*, 2020; Sowers *et al.*, 2020; Wingard *et al.*, 2021, 2021). The dietary regime employed in this study
506 has been well characterized as a model of diastolic dysfunction, with gradual development of metabolic
507 disturbance (stable rate of weight gain and mild hyperglycemia), with maintained systolic function (ejection
508 fraction and fractional shortening). The data presented here are consistent with clinical observations linking
509 cardiometabolic disease and diastolic dysfunction.
510
511 As we have reported previously, over the time span of the dietary intervention differential fibrosis is not
512 observed (Daniels *et al.*, 2022; Wells *et al.*, 2023). The finding of increased stiffness in cardiometabolic
513 disease is consistent with some aspects of prior experiments involving animal feeding of obesogenic diets,
514 using other rodent preparation types – including permeabilized cardiomyocytes, tissue strips/papillary
515 muscles, and non-paced cardiomyocytes (Leopoldo *et al.*, 2010; Gonçalves *et al.*, 2016; Sowers *et al.*, 2020).
516 Interestingly stiffness in those studies was attributed to titin or extracellular matrix properties. Our protocol
517 with intact single cardiomyocytes allows a mechanistic extension of these previous findings.
518
519 **Loading the intact cardiomyocyte - functional deficits revealed in HFSD**
520 Non-loaded contracting cardiomyocytes of CTRL and HFSD mice exhibited identical shortening-lengthening
521 cycles, but a distinctly different decrement in lengthening rate when exposed to load (i.e. auxotonic with
522 progressive 'pre-load' increase). Our findings show unequivocally that cardiomyocyte mechanical
523 dysfunction cannot be detected by analysis of non-loaded shortening. With loading, the shortening extent
524 and the maximal lengthening rates were reduced for both CTRL and HFSD. In HFSD the lengthening rate
525 reduction was accentuated even when shortening extent was accounted for. These findings indicated
526 specific influence of loading on lengthening in HFSD cardiomyocytes and could reflect impaired subcellular
527 relaxation processes specific to the HFSD myocardium.
528
529 Others have demonstrated a physiological effect of loading on shortening in cardiac cells/tissues in
530 different species (using slow pacing and sub physiologic temperature conditions), although the pronounced
531 effect on relaxation is not consistently reported (Lab *et al.*, 1984; White *et al.*, 1995; Shimkunas *et al.*,
532 2021). This is consistent with *in vivo* human clinical observations where there is a strong inverse association

533 between late-systolic loading and left ventricular wall displacement velocity during early diastole (Borlaug
534 *et al.*, 2007). Importantly, increased dependence of relaxation on after-load is reported to be an *in vivo*
535 feature of heart failure with diastolic dysfunction (Eichhorn *et al.*, 1992; Gillebert *et al.*, 2000). Regarding
536 the Ca^{2+} transient, in the current study a subtle prolongation effect is observed in both CTRL and HFSD
537 cardiomyocytes when loaded (but not stretched) which is consistent with recently reported findings in rat
538 LV trabeculae (Dowrick *et al.*, 2022). The variability in the sarcomere shortening recorded for both non-
539 loaded and loaded cardiomyocytes is notable (**Fig. 3**) but consistent with other studies assessing relaxation
540 of rodent cardiomyocytes (Delbridge & Roos, 1997; Clark & Campbell, 2019).
541
542 **Characterizing cardiomyocyte stretch & pacing challenge responses**
543 In order to quantify intact single cardiomyocyte stiffness our approach was to apply a calibrated stretch
544 protocol, based on pre-measurement of a stretch calibration constant for each myocyte, tracking changes
545 in force generation and cytosolic Ca^{2+} responses for each stretch step. This calibrated step-by-step
546 approach enabled the stress and strain data to be gathered from actively paced cardiomyocytes over
547 extended periods (i.e. 80-100sec) and computed to generate a definitive, comparative stiffness parameter
548 for each cardiomyocyte.
549
550 In the intact myocyte model, the internal cytosolic regulatory milieu is preserved, and the
551 cytoskeletal/sarcomeric/organelle structural framework is integral. Thus contributions to diastolic
552 'stiffness' reflect components of the structural passive resistance to deformation and the basal crossbridge-
553 derived activity. Recent studies of permeabilized cardiac muscle strip bundles have explored the separate
554 contributions of mictrotubule, titin, actin-associated, sarcolemmal and desmin-linked components to
555 passive force development (Loescher *et al.*, 2023). Prior studies of 'skinned' or quiescent myocardial
556 preparations have also identified sources of passive stiffness elevation, with titin isoform switch and
557 modification identified as major modulators of stiffness in cardiometabolic disease (Leopoldo *et al.*, 2010;
558 Hamdani *et al.*, 2013; Gonçalves *et al.*, 2016; Hopf *et al.*, 2018; Sowers *et al.*, 2020; Abdellatif *et al.*, 2021).
559
560 Our findings indicate involvement of a cytosolic Ca^{2+} component of the stretch response. Ca^{2+} fluorescence
561 analyses from these stretch protocols showed novel stretch-dependent prolongation of Ca^{2+} transient
562 decay in the HFSD cardiomyocytes. The time constant of Ca^{2+} transient decay increased with loading and
563 further with stretching – a feature not evident in CTRL cardiomyocytes and which provides additional
564 mechanistic insight .
565
566 The final pacing frequency protocol was implemented as a relative workload stress to the loaded
567 cardiomyocyte. With a doubling of pacing frequency, a significant increase in the stress/strain gradient was
568 observed in HFSD cardiomyocytes (and not CTRL), and a similar reduction in diastolic sarcomere length in

569 both CTRL and HFSD was observed. While cardiomyocyte diastolic Ca^{2+} level increased in both CTRL and
570 HFSD – the HFSD increase was less marked than CTRL. This was a surprising finding, not previously
571 reported in any other model setting. A suggestion of Ca^{2+} hyper-sensitivity arises (Davis *et al.*, 2007)
572 amongst other explanations to consider.
573
574 **Mechanistic insights into cross-bridge derived stiffness**
575 Here we report that a cardiometabolic disease phenotype induced by obesogenic diet includes a 70%
576 increase in cardiomyocyte stiffness which contributes to a 35% increase in diastolic dysfunction *in vivo* (by
577 echo E/e'). Several lines of evidence emerging from this study suggest that Ca^{2+} -related mechanism/s may
578 contribute to cardiomyocyte stiffness increase. Specifically, in the loaded HFSD cardiomyocyte (vs CTRL):
579 a) load confers accentuated lengthening rate deficit
580 b) with stretch, the Ca^{2+} transient decay time course is prolonged
581 c) with more rapid pacing, relatively small increases in diastolic Ca^{2+} are associated with elevated stiffness
582 Together these cardiomyocyte phenotypes would be consistent with selective impairment of relaxation
583 rate, selective myofilament hyper-activation, impeded diastolic filling and reduced diastolic reserve.
584
585 This combination of observations is consistent with the notion that stretch-dependent cross-bridge
586 attachment is prolonged in HFSD cardiomyocytes (or conversely detachment is delayed). We can speculate
587 that an alteration in the 3-dimensional geometry of the low affinity Ca^{2+} binding pocket in troponin C (TnC)
588 would produce this effect, by stabilizing Ca^{2+} in the pocket for longer every activation cycle. This could
589 increase TnC buffering power which would explain the relatively small Ca^{2+} rise in HFSD in response to
590 increased pacing (Eisner *et al.*, 2023). A manifestation of this altered binding function could be apparent
591 Ca^{2+} hypersensitivity. The TnC-Ca^{2+} dissociation rate has been theorized as an effector of the transient
592 decay time-course (Robinson *et al.*, 2018). A role for the troponin complex in regulation of Ca^{2+} affinity is
593 well established (Chemla *et al.*, 2000). Given the load and stretch-dependent nature of these findings, a
594 role for stress sensor proteins such as titin is likely. Indeed, there is some evidence to suggest that titin
595 isoform regulates TnC low-affinity binding pocket opening and Ca^{2+} affinity in response to stretch via
596 regulating the number of attached cross-bridges (Li *et al.*, 2019). Further evidence of structural
597 modifications of specific myofilament regions which form and regulate this pocket is required. Mass
598 spectrometry studies by us and others provide proof of concept of relevant post-translational modification
599 types (Janssens *et al.*, 2018; Loescher *et al.*, 2022).
600
601 **Limitations**
602 Given the diastolic dysfunction focus of this study, investigations have primarily examined cardiomyocyte
603 relaxation and lengthening behaviors. Diastolic and systolic interactions are important and additional
604 protocols are in development for these studies. In this regard, we defer to the extensive body of

technologic research undertaken to develop software and instrumentation to perform single cardiomyocyte 'Pressure-Volume (PV) loops' (Helmes *et al.*, 2016). Using this approach, to mimic PV cycles in the intact myocardium, stretch is applied after relaxation has occurred by using a force clamp to maintain a predefined diastolic force level. This approach has been used to discover that titin truncation shifts the working sarcomere length range preserving diastolic stiffness at the expense of systolic performance (Methawasin *et al.*, 2022) and that highly compliant titin allows cardiomyocytes to function at high diastolic Ca^{2+} levels (Najafi *et al.*, 2019). Potentially, this approach could also be used to evaluate the temporal relationship between slow or incomplete relaxation and cardiomyocyte cross-bridge derived stiffness in a semi-situ manner. Operator expertise is imperative with this system which to date has been very productive in the hands of the developers.

In our work we have adopted a pragmatic approach, simpler to implement – although still very challenging with about 20% non-loaded-to-loaded myocyte conversion success rate. When animals have many months of dietary treatment history, and as cell isolation from older and diseased hearts is difficult, an optimized loading and stretching approach is key. The two approaches have not been benchmarked, although it can be predicted that the viscous components of stiffness are likely underestimated when stretches are slow and relatively small such as in the current study (Caporizzo & Prosser, 2021). The capacity to directly and reproducibly determine Youngs Modulus (stress/strain) with a slow stretch routine has useful comparative value.

With ongoing research, a priority is to undertake longitudinal studies, including both sexes, to investigate the relative timing of the emergence of *in vivo* and *in vitro* stiffness phenotypes as differences in Ca^{2+} handling have previously been observed between control male and female rodents (Farrell *et al.*, 2010). This has high translational relevance as we have previously identified a differential time course of diastolic dysfunction emergence in females and males, with increased female vulnerability (Reichelt *et al.*, 2013; Chandramouli *et al.*, 2018).

In conclusion

This is the first study to link elevated intact single cardiomyocyte stiffness with *in vivo* diastolic dysfunction in a dietary acquired cardiometabolic disease mouse model. The novel findings identify augmented load dependent TnC-Ca^{2+} interactions as one potential feature of myofilament function which contributes to cardiomyocyte stiffness in hearts exhibiting cardiometabolic diastolic dysfunction. Taken together, the findings emphasize the importance of mechanical loading and pacing frequency in revealing latent diastolic abnormalities at the cardiomyocyte level. The rationale for further studies identifying specific subcellular and molecular mechanisms of cardiomyocyte stiffness in cardiometabolic disease prior to failure onset is compelling.

641 **ADDITIONAL INFORMATION**

642

643 **Data availability statement**

644 The data that support the findings of this study are available from the corresponding author upon
645 reasonable request.

646

647 **Competing interests**

648 The authors declare that they have no competing interests.

649

650 **Author contributions**

651 All experiments were performed at the Cardiac Phenomics Laboratory at the University of Melbourne,
652 Australia. J.V.J., K.M.M. and L.M.D.D. contributed to the conception and research design of the work. All
653 authors contributed to the acquisition, analysis or interpretation of data for the work and contributed to
654 drafting the work or revising it critically for important intellectual content. All authors provide final
655 approval of the version to be published and agreement to be accountable for all aspects of the work.

656

657 **Funding**

658 This work was supported by grants from the National Health and Medical Research Council of Australia
659 (LMDD: NHMRCA 1157320), the Diabetes Australia Research Trust (LMDD), the National Heart Foundation
660 of Australia (LMDD: NHFA), the New Zealand Marsden Fund (KMM: 19-UOA-268), the Health Research
661 Council of New Zealand (KMM:19/190), and the National Institutes of Health USA (JVE: R01 HL155346-01 &
662 R01 HL144509-01).

663

664

665 **REFERENCES**

666 Abdellatif M et al. (2021). Nicotinamide for the treatment of heart failure with preserved ejection fraction.
667 *Sci Transl Med* **13,** eabd7064.

668 Aurigemma GP, Zile MR & Gaasch WH (2006). Contractile Behavior of the Left Ventricle in Diastolic Heart
669 Failure. *Circulation* **113,** 296–304.

670 Borlaug BA, Melenovsky V, Redfield MM, Kessler K, Chang H-J, Abraham TP & Kass DA (2007). Impact of
671 Arterial Load and Loading Sequence on Left Ventricular Tissue Velocities in Humans. *Journal of the*
672 *American College of Cardiology* **50,** 1570–1577.

673 Caporizzo MA & Prosser BL (2021). Need for Speed: The Importance of Physiological Strain Rates in
674 Determining Myocardial Stiffness. *Front Physiol* **12,** 696694.

675 Chandramouli C, Reichelt ME, Curl CL, Varma U, Bienvenu LA, Koutsifeli P, Raaijmakers AJA, De Blasio MJ,
676 Qin CX, Jenkins AJ, Ritchie RH, Mellor KM & Delbridge LMD (2018). Diastolic dysfunction is more
677 apparent in STZ-induced diabetic female mice, despite less pronounced hyperglycemia. *Sci Rep* **8,**
678 2346.

679 Chemla D, Coirault C, Hébert J-L & Lecarpentier Y (2000). Mechanics of Relaxation of the Human Heart.
680 *Physiology* **15,** 78–83.

681 Clark JA & Campbell SG (2019). Diverse relaxation rates exist among rat cardiomyocytes isolated from a
682 single myocardial region. *J Physiol* **597,** 711–722.

683 Curl CL, Danes VR, Bell JR, Raaijmakers AJA, Ip WTK, Chandramouli C, Harding TW, Porrello ER, Erickson JR,
684 Charchar FJ, Kompa AR, Edgley AJ, Crossman DJ, Soeller C, Mellor KM, Kalman JM, Harrap SB &
685 Delbridge LMD (2018). Cardiomyocyte Functional Etiology in Heart Failure With Preserved Ejection
686 Fraction Is Distinctive-A New Preclinical Model. *J Am Heart Assoc* **7,** e007451.

687 Daniels LJ, Macindoe C, Koutsifeli P, Annandale M, Raaijmakers AJA, Weeks KL, Bell JR, Janssens JV, Curl CL,
688 Delbridge LMD & Mellor KM (2022). Myocardial deformation imaging by 2D speckle tracking
689 echocardiography for assessment of diastolic dysfunction in murine cardiopathology.
690 2022.08.06.503061. Available at: https://www.biorxiv.org/content/10.1101/2022.08.06.503061v1
691 [Accessed May 21, 2023].

692 Davis J, Wen H, Edwards T & Metzger JM (2007). Thin Filament Disinhibition by Restrictive Cardiomyopathy
693 Mutant R193H Troponin I Induces Ca2+-Independent Mechanical Tone and Acute Myocyte
694 Remodeling. *Circulation Research* **100,** 1494–1502.

695 Delbridge LM & Roos KP (1997). Optical methods to evaluate the contractile function of unloaded isolated
696 cardiac myocytes. *J Mol Cell Cardiol* **29,** 11–25.

697 Delbridge LMD, Bell JR, Weeks KL, Raaijmakers AJA & Mellor KM (2022). HFpEF etiology - Can focus on sex-
698 specific mechanisms deliver insights for all? *J Mol Cell Cardiol* **173,** 71–72.

699 Dia M, Gomez L, Thibault H, Tessier N, Leon C, Chouabe C, Ducreux S, Gallo-Bona N, Tubbs E, Bendridi N,
700 Chanon S, Leray A, Belmudes L, Couté Y, Kurdi M, Ovize M, Rieusset J & Paillard M (2020). Reduced
701 reticulum–mitochondria Ca2+ transfer is an early and reversible trigger of mitochondrial
702 dysfunctions in diabetic cardiomyopathy. *Basic Res Cardiol* **115,** 74.

703 Dowrick JM, Tran K, Garrett AS, Anderson AJ, Nielsen PMF, Taberner AJ & Han J-C (2022). Work-loop
704 contractions reveal that the afterload-dependent time course of cardiac Ca2+ transients is
705 modulated by preload. *Journal of Applied Physiology* **133,** 663–675.

706 Eichhorn EJ, Willard JE, Alvarez L, Kim AS, Glamann DB, Risser RC & Grayburn PA (1992). Are contraction
707 and relaxation coupled in patients with and without congestive heart failure? *Circulation* **85,** 2132–
708 2139.

709 Eisner D, Neher E, Taschenberger H & Smith G (2023). Physiology of intracellular calcium buffering.
710 *Physiological Reviews* **103,** 2767–2845.

711 Eisner DA, Caldwell JL, Trafford AW & Hutchings DC (2020). The Control of Diastolic Calcium in the Heart.
712 *Circ Res* **126,** 395–412.

713 Fabiato A & Fabiato F (1978). Myofilament-generated tension oscillations during partial calcium activation
714 and activation dependence of the sarcomere length-tension relation of skinned cardiac cells. *J Gen*
715 *Physiol* **72,** 667–699.

716 Farrell SR, Ross JL & Howlett SE (2010). Sex differences in mechanisms of cardiac excitation-contraction
717 coupling in rat ventricular myocytes. *Am J Physiol Heart Circ Physiol* **299,** H36-45.

718 Fowler ED, Benoist D, Drinkhill MJ, Stones R, Helmes M, Wüst RCI, Stienen GJM, Steele DS & White E (2015).
719 Decreased creatine kinase is linked to diastolic dysfunction in rats with right heart failure induced
720 by pulmonary artery hypertension. *J Mol Cell Cardiol* **86,** 1–8.

721 Gillebert TC, Leite-Moreira AF & De Hert SG (2000). Load dependent diastolic dysfunction in heart failure.
722 *Heart Fail Rev* **5,** 345–355.

723 Gonçalves N, Silva AF, Rodrigues PG, Correia E, Moura C, Eloy C, Roncon-Albuquerque R, Falcão-Pires I &
724 Leite-Moreira AF (2016). Early cardiac changes induced by a hypercaloric Western-type diet in
725 "subclinical" obesity. *American Journal of Physiology-Heart and Circulatory Physiology* **310,** H655–
726 H666.

727 Hamdani N, Franssen C, Lourenço A, Falcão-Pires I, Fontoura D, Leite S, Plettig L, López B, Ottenheijm CA,
728 Becher PM, González A, Tschöpe C, Díez J, Linke WA, Leite-Moreira AF & Paulus WJ (2013).
729 Myocardial Titin Hypophosphorylation Importantly Contributes to Heart Failure With Preserved
730 Ejection Fraction in a Rat Metabolic Risk Model. *Circulation: Heart Failure* **6,** 1239–1249.

731 Heather LC, Hafstad AD, Halade GV, Harmancey R, Mellor KM, Mishra PK, Mulvihill EE, Nabben M,
732 Nakamura M, Rider OJ, Ruiz M, Wende AR & Ussher JR (2022). Guidelines on models of diabetic
733 heart disease. *Am J Physiol Heart Circ Physiol* **323,** H176–H200.

734 Helmes M, Najafi A, Palmer BM, Breel E, Rijnveld N, Iannuzzi D & van der Velden J (2016). Mimicking the
735 cardiac cycle in intact cardiomyocytes using diastolic and systolic force clamps; measuring power
736 output. *Cardiovasc Res* **111,** 66–73.

737 Hopf A-E, Andresen C, Kötter S, Isić M, Ulrich K, Sahin S, Bongardt S, Röll W, Drove F, Scheerer N,
738 Vandekerckhove L, De Keulenaer GW, Hamdani N, Linke WA & Krüger M (2018). Diabetes-Induced
739 Cardiomyocyte Passive Stiffening Is Caused by Impaired Insulin-Dependent Titin Modification and
740 Can Be Modulated by Neuregulin-1. *Circulation Research* **123,** 342–355.

741 Howlett SE, Grandy SA & Ferrier GR (2006). Calcium spark properties in ventricular myocytes are altered in
742 aged mice. *American Journal of Physiology-Heart and Circulatory Physiology* **290,** H1566–H1574.

743 Jackson AM et al. (2022). Diabetes and pre-diabetes in patients with heart failure and preserved ejection
744 fraction. *Eur J Heart Fail* **24,** 497–509.

745 Janssens JV, Ma B, Brimble MA, Van Eyk JE, Delbridge LMD & Mellor KM (2018). Cardiac troponins may be
746 irreversibly modified by glycation: novel potential mechanisms of cardiac performance modulation.
747 *Sci Rep* **8,** 16084.

748 Janssens JV, Raaijmakers AJA, Weeks KL, Bell JR, Mellor KM, Curl CL & Delbridge LMD (2024). The
749 cardiomyocyte origins of diastolic dysfunction: cellular components of myocardial stiffness. *Am J*
750 *Physiol Heart Circ Physiol*; DOI: 10.1152/ajpheart.00334.2023.

751 Kamon T, Kaneko H, Itoh H, Kiriyama H, Koyama K, Fujiu K, Morita H, Uno K, Hayashi N & Komuro I (2020).
752 Association between insulin resistance and left ventricular diastolic dysfunction in non-diabetic
753 general population. *European Heart Journal* **41,** ehaa946.3057.

754 Kilfoil PJ, Lotteau S, Zhang R, Yue X, Aynaszyan S, Solymani RE, Cingolani E, Marbán E & Goldhaber JI (2020).
755 Distinct features of calcium handling and β-adrenergic sensitivity in heart failure with preserved
756 versus reduced ejection fraction. *J Physiol* **598,** 5091–5108.

757 Kittleson MM, Panjrath GS, Amancherla K, Davis LL, Deswal A, Dixon DL, Januzzi JL & Yancy CW (2023). 2023
758 ACC Expert Consensus Decision Pathway on Management of Heart Failure With Preserved Ejection
759 Fraction: A Report of the American College of Cardiology Solution Set Oversight Committee. *Journal*
760 *of the American College of Cardiology* **81,** 1835–1878.

761 Lab MJ, Allen DG & Orchard CH (1984). The effects of shortening on myoplasmic calcium concentration and
762 on the action potential in mammalian ventricular muscle. *Circulation Research* **55,** 825–829.

763 Lam CSP, Arnott C, Beale AL, Chandramouli C, Hilfiker-Kleiner D, Kaye DM, Ky B, Santema BT, Sliwa K &
764 Voors AA (2019). Sex differences in heart failure. *European Heart Journal* **40,** 3859–3868c.

765 Leopoldo AS, Sugizaki MM, Lima-Leopoldo AP, do Nascimento AF, de Azevedo Melo Luvizotto R, de Campos
766 DHS, Okoshi K, Pai-Silva MD, Padovani CR & Cicogna AC (2010). Cardiac remodeling in a rat model
767 of diet-induced obesity. *Can J Cardiol* **26,** 423–429.

768 Leung M, Phan V, Whatmough M, Heritier S, Wong VW & Leung DY (2015). Left ventricular diastolic reserve
769 in patients with type 2 diabetes mellitus. *Open Heart* **2,** e000214.

770 Li K-L, Methawasin M, Tanner BCW, Granzier HL, Solaro RJ & Dong W-J (2019). Sarcomere length–
771 dependent effects on Ca2+-troponin regulation in myocardium expressing compliant titin. *J Gen*
772 *Physiol* **151,** 30–41.

773 Llano-Diez M, Sinclair J, Yamada T, Zong M, Fauconnier J, Zhang S-J, Katz A, Jardemark K, Westerblad H,
774 Andersson DC & Lanner JT (2016). The Role of Reactive Oxygen Species in β-Adrenergic Signaling in
775 Cardiomyocytes from Mice with the Metabolic Syndrome. *PLoS One* **11,** e0167090.

776 Lo Q & Thomas L (2010). Echocardiographic evaluation of diastolic heart failure. *Australas J Ultrasound Med*
777 **13,** 14–26.

778 Loescher CM, Freundt JK, Unger A, Hessel AL, Kühn M, Koser F & Linke WA (2023). Titin governs myocardial
779 passive stiffness with major support from microtubules and actin and the extracellular matrix. *Nat*
780 *Cardiovasc Res* **2,** 991–1002.

781 Loescher CM, Hobbach AJ & Linke WA (2022). Titin (TTN): from molecule to modifications, mechanics, and
782 medical significance. *Cardiovascular Research* **118,** 2903–2918.

783 Louch WE (2020). A horse of a different colour: distinct mechanisms of HFpEF and HFrEF. *J Physiol* **598,**
784 5005–5006.

785 McHugh K, DeVore AD, Wu J, Matsouaka RA, Fonarow GC, Heidenreich PA, Yancy CW, Green JB, Altman N
786 & Hernandez AF (2019). Heart Failure With Preserved Ejection Fraction and Diabetes: JACC State-
787 of-the-Art Review. *J Am Coll Cardiol* **73,** 602–611.

788 Mellor KM, Bell JR, Young MJ, Ritchie RH & Delbridge LMD (2011). Myocardial autophagy activation and
789 suppressed survival signaling is associated with insulin resistance in fructose-fed mice. *Journal of*
790 *Molecular and Cellular Cardiology* **50,** 1035–1043.

791 Mellor KM, Wendt IR, Ritchie RH & Delbridge LMD (2012). Fructose diet treatment in mice induces
792 fundamental disturbance of cardiomyocyte Ca2+ handling and myofilament responsiveness. *Am J*
793 *Physiol Heart Circ Physiol* **302,** H964-972.

794 Methawasin M, Farman GP, Granzier-Nakajima S, Strom J, Kiss B, Smith JE & Granzier H (2022). Shortening
795 the thick filament by partial deletion of titin's C-zone alters cardiac function by reducing the
796 operating sarcomere length range. *J Mol Cell Cardiol* **165,** 103–114.

797 Mirsky I (1976). Assessment of passive elastic stiffness of cardiac muscle: mathematical concepts,
798 physiologic and clinical considerations, directions of future research. *Prog Cardiovasc Dis* **18,** 277–
799 308.

800 Najafi A, van de Locht M, Schuldt M, Schönleitner P, van Willigenburg M, Bollen I, Goebel M, Ottenheijm
801 CAC, van der Velden J, Helmes M & Kuster DWD (2019). End-diastolic force pre-activates
802 cardiomyocytes and determines contractile force: role of titin and calcium. *J Physiol* **597,** 4521–
803 4531.

804 Natali AJ, Turner DL, Harrison SM & White E (2001). Regional effects of voluntary exercise on cell size and
805 contraction-frequency responses in rat cardiac myocytes. *Journal of Experimental Biology* **204,**
806 1191–1199.

807 Patil VC, Patil HV, Shah KB, Vasani JD & Shetty P (2011). Diastolic dysfunction in asymptomatic type 2
808 diabetes mellitus with normal systolic function. *J Cardiovasc Dis Res* **2,** 213–222.

809 Peyronnet R, Bollensdorff C, Capel RA, Rog-Zielinska EA, Woods CE, Charo DN, Lookin O, Fajardo G, Ho M,
810 Quertermous T, Ashley EA & Kohl P (2017). Load-dependent effects of apelin on murine
811 cardiomyocytes. *Prog Biophys Mol Biol* **130,** 333–343.

812 Pulinilkunnil T, Kienesberger PC, Nagendran J, Sharma N, Young ME & Dyck JRB (2014). Cardiac-specific
813 adipose triglyceride lipase overexpression protects from cardiac steatosis and dilated
814 cardiomyopathy following diet-induced obesity. *Int J Obes* **38,** 205–215.

815 Redfield MM (2016). Heart Failure with Preserved Ejection Fraction. *N Engl J Med* **375,** 1868–1877.

816 Reichelt ME, Mellor KM, Bell JR, Chandramouli C, Headrick JP & Delbridge LMD (2013). Sex, sex steroids,
817 and diabetic cardiomyopathy: making the case for experimental focus. *Am J Physiol Heart Circ*
818 *Physiol* **305,** H779-792.

819 Robinson P, Liu X, Sparrow A, Patel S, Zhang Y-H, Casadei B, Watkins H & Redwood C (2018). Hypertrophic
820 cardiomyopathy mutations increase myofilament Ca2+ buffering, alter intracellular Ca2+ handling,
821 and stimulate Ca2+-dependent signaling. *J Biol Chem* **293,** 10487–10499.

822 Rozenbaum Z, Topilsky Y, Khoury S, Pereg D & Laufer-Perl M (2019). Association of body mass index and
823 diastolic function in metabolically healthy obese with preserved ejection fraction. *Int J Cardiol* **277,**
824 147–152.

825 Saad NS, Mashali MA, Repas SJ & Janssen PML (2023). Altering Calcium Sensitivity in Heart Failure: A
826 Crossroads of Disease Etiology and Therapeutic Innovation. *Int J Mol Sci* **24,** 17577.

827 Satoh H, Delbridge LM, Blatter LA & Bers DM (1996). Surface:volume relationship in cardiac myocytes
828 studied with confocal microscopy and membrane capacitance measurements: species-dependence
829 and developmental effects. *Biophys J* **70,** 1494–1504.

830 Shimkunas R et al. (2021). Mechanical Load Regulates Excitation-Ca2+ Signaling-Contraction in
831 Cardiomyocyte. *Circ Res* **128,** 772–774.

832 Sotomi Y et al. (2021). Sex Differences in Heart Failure With Preserved Ejection Fraction. *J Am Heart Assoc*
833 **10,** e018574.

834 Sowers JR, Habibi J, Jia G, Bostick B, Manrique-Acevedo C, Lastra G, Yang Y, Chen D, Sun Z, Domeier TL,
835 Durante W, Whaley-Connell AT, Hill MA, Jaisser F, DeMarco VG & Aroor AR (2020). Endothelial
836 sodium channel activation promotes cardiac stiffness and diastolic dysfunction in Western diet fed
837 female mice. *Metabolism* **109,** 154223.

838 Varian KD & Janssen PML (2007). Frequency-dependent acceleration of relaxation involves decreased
839 myofilament calcium sensitivity. *American Journal of Physiology-Heart and Circulatory Physiology*
840 **292,** H2212–H2219.

841 Villalobos Lizardi JC, Baranger J, Nguyen MB, Asnacios A, Malik A, Lumens J, Mertens L, Friedberg MK,
842 Simmons CA, Pernot M & Villemain O (2022). A guide for assessment of myocardial stiffness in
843 health and disease. *Nat Cardiovasc Res* **1,** 8–22.

844 Wang Q, Wang Y, West TM, Liu Y, Reddy GR, Barbagallo F, Xu B, Shi Q, Deng B, Wei W & Xiang YK (2020).
845 Carvedilol induces biased β1 adrenergic receptor-Nitric oxide synthase 3-cyclic guanylyl
846 monophosphate signaling to promote cardiac contractility. *Cardiovasc Res*cvaa266.

847 Wells SP, Raaijmakers AJA, Curl CL, O'Shea C, Hayes S, Mellor KM, Kalman JM, Kirchhof P, Pavlovic D,
848 Delbridge LMD & Bell JR (2023). Localized cardiomyocyte lipid accumulation is associated with
849 slowed epicardial conduction in rats. *J Gen Physiol* **155,** e202213296.

850 West TM, Wang Q, Deng B, Zhang Y, Barbagallo F, Reddy GR, Chen D, Phan KS, Xu B, Isidori A & Xiang YK
851 (2019). Phosphodiesterase 5 Associates With β2 Adrenergic Receptor to Modulate Cardiac Function
852 in Type 2 Diabetic Hearts. *JAHA*; DOI: 10.1161/JAHA.119.012273.

853 White E, Boyett MR & Orchard CH (1995). The effects of mechanical loading and changes of length on single
854 guinea-pig ventricular myocytes. *The Journal of Physiology* **482,** 93–107.

855 Wingard MC, Dalal S, Shook PL, Myers R, Connelly BA, Thewke DP, Singh M & Singh K (2021). Deficiency of
856 ataxia-telangiectasia mutated kinase modulates functional and biochemical parameters of the
857 heart in response to Western-type diet. *Am J Physiol Heart Circ Physiol* **320,** H2324–H2338.

858 Zhou P & Pu WT (2016). Recounting Cardiac Cellular Composition. *Circulation Research* **118,** 368–370.

859

860 **FIGURE LEGENDS**

861 **Fig.1 Systemic indicators of cardiometabolic disease and *in vivo* diastolic function in high fat/sugar diet**
862 **(HFSD) vs control (CTRL) mice**.
863 **A**. Body weight elevation at 5 week intervals up to 25 weeks of dietary treatment (last timepoint full cohort
864 intact. N = 16 – 17 mice per group).
865 **B.** Glucose tolerance testing at 23-24 weeks post dietary intervention; N = 6 mice per group).
866 **C**. Echocardiography exemplar blood flow and tissue doppler images from which diastolic indices were
867 derived for CTRL and HFSD mice. Upper panels: HFSD mitral blood flow & annular wall motion. Lower
868 panels: CTRL mitral blood flow & annular wall motion. (N = 9-16 mice per group)
869 **D**. Early diastolic mitral annular blood flow (E) was increased in HFSD.
870 **E.** Early diastolic mitral annular wall velocity (e') was decreased in HFSD.
871 **F.** Deceleration time of early diastolic mitral annular blood flow was decreased in HFSD.
872 **G.** Ratio of early diastolic blood flow to wall velocity (E/e') was increased in HFSD.
873
874 Time-course data analysed using two-way repeated measures ANOVA with Sidak post-hoc test (*$p < 0.05$).
875 Comparisons between two treatment groups performed using student's t-test; *$p<0.05$, **$p<0.01$,
876 ***$p<0.001$). Data presented as mean ± standard error of the mean.
877
878
879 **Fig.2 Non-loaded sarcomere and Ca^{2+} dynamics in CTRL and HFSD cardiomyocytes.**
880 **A.** Mean sarcomere contraction cycles presented as a percentage of diastolic sarcomere length for CTRL
881 and HFSD cardiomyocytes
882 **B-C.** Mean diastolic sarcomere length and extent of sarcomere shortening for CTRL and HFSD
883 cardiomyocytes.
884 **D.** Mean sarcomere shortening and lengthening rate records (time derivative of sarcomere contraction-
885 relaxation cycle) for CTRL and HFSD cardiomyocytes. The nadir and zenith represent maximal shortening
886 and lengthening rates respectively.
887 **E-F.** Maximal rate of lengthening and shortening rates for CTRL and HFSD cardiomyocytes.
888 **G.** Mean Ca^{2+} transient records for CTRL and HFSD cardiomyocytes.
889 **H-J.** Mean Ca^{2+} levels (systolic and diastolic) and time constant of transient decay (*tau*) in HFSD and CTRL
890 cardiomyocytes.
891
892 Mean data computed from average of 20 cycles per cardiomyocyte to derive group mean (N = 6-8 mice per
893 group, n = 32-49 cells per group). Comparisons between two treatment groups performed using student's
894 t-test (all $p>0.05$, ns). Data presented as mean ± standard error of the mean.
895

896 **Fig. 3 Sarcomere shortening and lengthening in non-loaded and loaded pacing states.**
897 **A.** Exemplar non-loaded and loaded sarcomere contraction cycles for the same cardiomyocyte (CTRL).
898 **B-C.** Extent of sarcomere shortening and maximum rate of lengthening, measured for each cardiomyocyte
899 in non-loaded and loaded state for CTRL and HFSD groups combined (N = 9 mice, n = 25 cells). Mean data
900 for CTRL and HFSD are presented as grey points to the left (non-loaded) and right (loaded) of individual
901 cardiomyocyte data.
902 **D.** Correlation of loading associated sarcomere shortening change and maximum rate of lengthening
903 change for CTRL and HFSD combined.
904 **E.** Mean sarcomere loading effect on maximum deformation rate during lengthening ((µm/s) / (µm);
905 maximum rate of lengthening (µm/s) normalized by shortening extent (µm)) for CTRL vs HFSD. (CTRL: N = 5
906 mice, n = 13 cells; HFSD: N = 4 mice, n = 12 cells). Significant ANOVA interaction effect (diet treatment x
907 load state).
908 **F.** Mean decrement in deformation rate during lengthening ((µm/s) / (µm)).
909
910 Comparison of cardiomyocyte responses in different loading conditions analysed by paired t-test.
911 Comparison of cardiomyocytes from different treatment groups analysed by unpaired t-test. A 2-way
912 ANOVA with repeated measures used for analysis of two independent variables. Data fitted with linear
913 regression model and calculation of Pearson's correlation coefficient. Data presented as mean ± standard
914 error of the mean. *p<0.05, **p<0.01, ****p<0.0001, #p<0.05 ANOVA factor interaction.
915
916
917 **Fig. 4 Quantifying diastolic stiffness in CTRL vs HFSD cardiomyocytes using strain normalization methods**
918 **A.** Exemplar stress recordings of CTRL and HFSD cardiomyocytes undergoing 'stress-length' protocol (2Hz
919 paced). Diastolic baseline stress shifts indicated by broken line.
920 **B.** Diastolic and systolic sarcomere mean stress- sarcomere length (SL) relations in CTRL cardiomyocytes (N
921 = 5 mice, n = 9 cells).
922 **C.** Diastolic mean stress-sarcomere length relation (linear regression fit) for HFSD and CTRL.
923 **D.** Diastolic stress (mN/mm^2) normalized relative to sarcomere stretch (µm) yields sarcomere stress/strain =
924 stiffness [(mN/mm^2) /strain (µm)] for HFSD and CTRL.
925 **E.** Diastolic mean cardiomyocyte segment stress-length relation (linear regression fit) for HFSD and CTRL.
926 **F.** Diastolic stress (mN/mm^2) normalized relative to segment stretch (% length) yields cardiomyocyte
927 segment stress/strain = stiffness [(mN/mm^2) /strain (% length)] for HFSD & CTRL.
928 **G.** Correlation (linear regression fit) of *in vitro* cardiomyocyte segment diastolic stiffness (stress/strain) with
929 *in vivo* diastolic dysfunction E/e' (blood flow/wall motion) in CTRL and HFSD. Cardiomyocyte data averaged
930 per heart.
931
932 Comparisons between two groups performed using student's t-test (*p<0.05, **p<0.01). Data fitted with
933 linear regression model and calculation of Pearson's correlation coefficient, presented as mean ± standard
934 error of the mean. For A. & B. (CTRL: N=5 mice, n=9 cells; HFSD: N=2 mice, n=7 cells). For C.&D. (CTRL: N=6
935 mice, n = 16 cells; HFSD: N=6 mice, n=18 cells).
936

Fig. 5 Load dependence of cardiomyocyte Ca^{2+} transient decay in CTRL and HFSD cardiomyocytes.
A. Time constant of Ca^{2+} transient decay (tau) in cardiomyocytes with different load conditions: loaded (L) & stretched (S) shown as fold change relative to non-loaded (N) for CTRL and HFSD.
B-C. Exemplar Ca^{2+} transient decay records, with a mono-exponential decay function fit, in non-loaded and stretched CTRL and HFSD cardiomyocytes. Horizontal black broken lines intersect with mono-exponential fit at 36.8% (1/e) transient amplitude. Vertical broken lines from intersection points indicate the time constant of Ca^{2+} transient decay (tau).

For analysis of two independent variables a 2-way ANOVA with repeated measures used (CTRL: N = 5 mice, n = 13 cells; HFSD: N = 4 mice, n = 12 cells). Data are presented as mean ± standard error of the mean. ***p<0.001 (HFSD stretched vs non-loaded). Non-significant ANOVA interaction effect (p = 0.055, diet treatment x load state).

Fig. 6 Pacing induced changes in cardiomyocyte cytosolic Ca^{2+} levels and stiffness in CTRL & HFSD.
A. Exemplar CTRL and HFSD cardiomyocyte Ca^{2+} transients at 2 and 4 Hz pacing.
B. Diastolic cardiomyocyte Ca^{2+} levels measured before and after transition from 2 to 4 Hz pacing in HFSD & CTRL.
C. Diastolic cardiomyocyte Ca^{2+} level mean shift with transition from 2 to 4 Hz pacing in HFSD & CTRL.
D. Diastolic sarcomere length measured before and after transition from 2 to 4 Hz pacing in HFSD & CTRL.
E. Diastolic mean cardiomyocyte segment stress-length relation (linear regression fit) for HFSD and CTRL at 2 and 4 Hz pacing.
F. Diastolic mean cardiomyocyte segment stress-length relation slope (mN/mm^2) normalized relative to segment stretch (% length) yields cardiomyocyte mean segment stress/strain = stiffness [(mN/mm^2) /strain (% length)] for HFSD and CTRL at 2 and 4 Hz pacing.

Comparison between two groups performed using unpaired t-test. With two independent variables a repeated measures 2-way ANOVA Sidaks post-hoc analysis was performed (*p<0.05, **p<0.01, ****p<0.0001). Data are presented as mean ± standard error of the mean or mean with paired individual points. For **B. & C.** (CTRL: N = 4 mice, n = 9 cells; HFSD: N = 4 mice, n = 8 cells). For **D. & E.** (CTRL: N = 4 mice, n = 7 cells; HFSD: N = 4 mice, n = 9 cells). For **F.** (CTRL: N = 4 mice, n = 8 cells; HFSD: N = 4 mice, n = 9 cells).

969 **Table S1. Echocardiographic parameters in CTRL and HFSD mice.**
970 *LVIDd* left ventricular internal diameter at end diastole, *IVSd* interventricular septum diameter at end
971 diastole, *LVPWd* left ventricular posterior wall thickness at end diastole, *RWT* relative wall thickness, *E*
972 *wave* mitral valve blood flow velocity during the early ventricular filling phase, *A wave* mitral valve blood
973 flow velocity during atrial contraction, *e' wave* mitral annulus tissue motion velocity during the early
974 ventricular filling phase, *a' wave* mitral annulus tissue motion velocity during atrial contraction, *MV Dec T*
975 mitral valve deceleration time.
976
977 Comparisons between two treatment groups performed using Students' unpaired t-test (N = 9-15 mice per
978 group; *p < 0.05, **p<0.01, ***p<0.001). Data are presented as mean ± standard error of the mean.
979
980
981 **Fig. S1. Cardiomyocyte standardized stretch protocol.**
982 **A.** Image of a left ventricular cardiomyocyte longitudinally attached to glass rods. Edge-tracking used to
983 measure inter-rod distance (marked as blue bars) for cardiomyocyte segment analyses. The delineated
984 region of interest (marked pink) represents the area from which Fast Fourier Transform analysis of
985 sarcomere striations was performed to derive sarcomere-specific data.
986 **B.** Exemplar traces depict the change in glass rod internal distance in response to successive 0.5V piezo-
987 motor inputs used for calibration of stretch protocol for each individual cardiomyocyte to allow normalized
988 comparisons.
989 **C.** Measuring stress and strain during progressive cardiomyocyte stretch. Exemplar force, sarcomere length
990 and rod edge-tracker traces during the first stretch of a stress-length protocol.
991 **D.** Comparison of variability of cell stretches performed using a uniform (preset) stretch constant and the
992 individually derived stretch calibration constant. Reproducibility is optimized using the individual stretch
993 calibration constant. Data shown as median ± interquartile range.

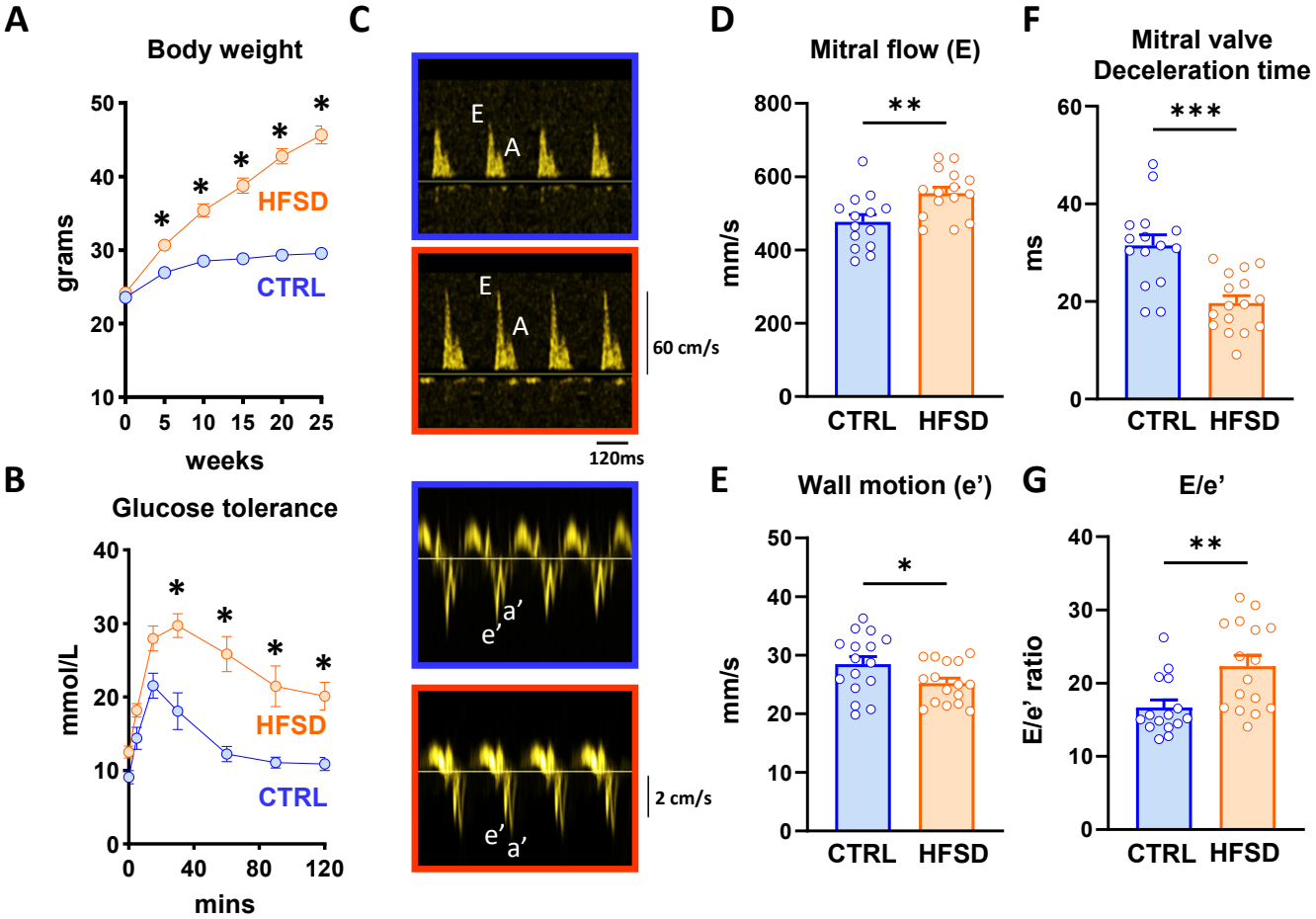

Fig.1 Systemic indicators of cardiometabolic disease and *in vivo* diastolic function in high-fat/sugar diet (HFSD) vs control (CTRL) mice.

A. Body weight elevation at 5 week intervals up to 25 weeks of dietary treatment (last timepoint full cohort intact. N = 16 – 17 mice per group).

B. Glucose tolerance testing at 23-24 weeks post dietary intervention; N = 6 mice per group).

C. Echocardiography exemplar blood flow and tissue doppler images from which diastolic indices were derived for CTRL and HFSD mice. Upper panels: HFSD mitral blood flow & annular wall motion. Lower panels: CTRL mitral blood flow & annular wall motion. (N = 14-16 mice per group)

D. Early diastolic mitral annular blood flow (E) was increased in HFSD.

E. Early diastolic mitral annular wall velocity (e') was decreased in HFSD.

F. Deceleration time of early diastolic mitral annular blood flow was decreased in HFSD.

G. Ratio of early diastolic blood flow to wall velocity (E/e') was increased in HFSD.

Time-course data analysed using two-way repeated measures ANOVA with Sidak post-hoc test (*$p < 0.05$). Comparisons between two treatment groups performed using student's t-test; *$p<0.05$, **$p<0.01$, ***$p<0.001$). Data presented as mean ± standard error of the mean.

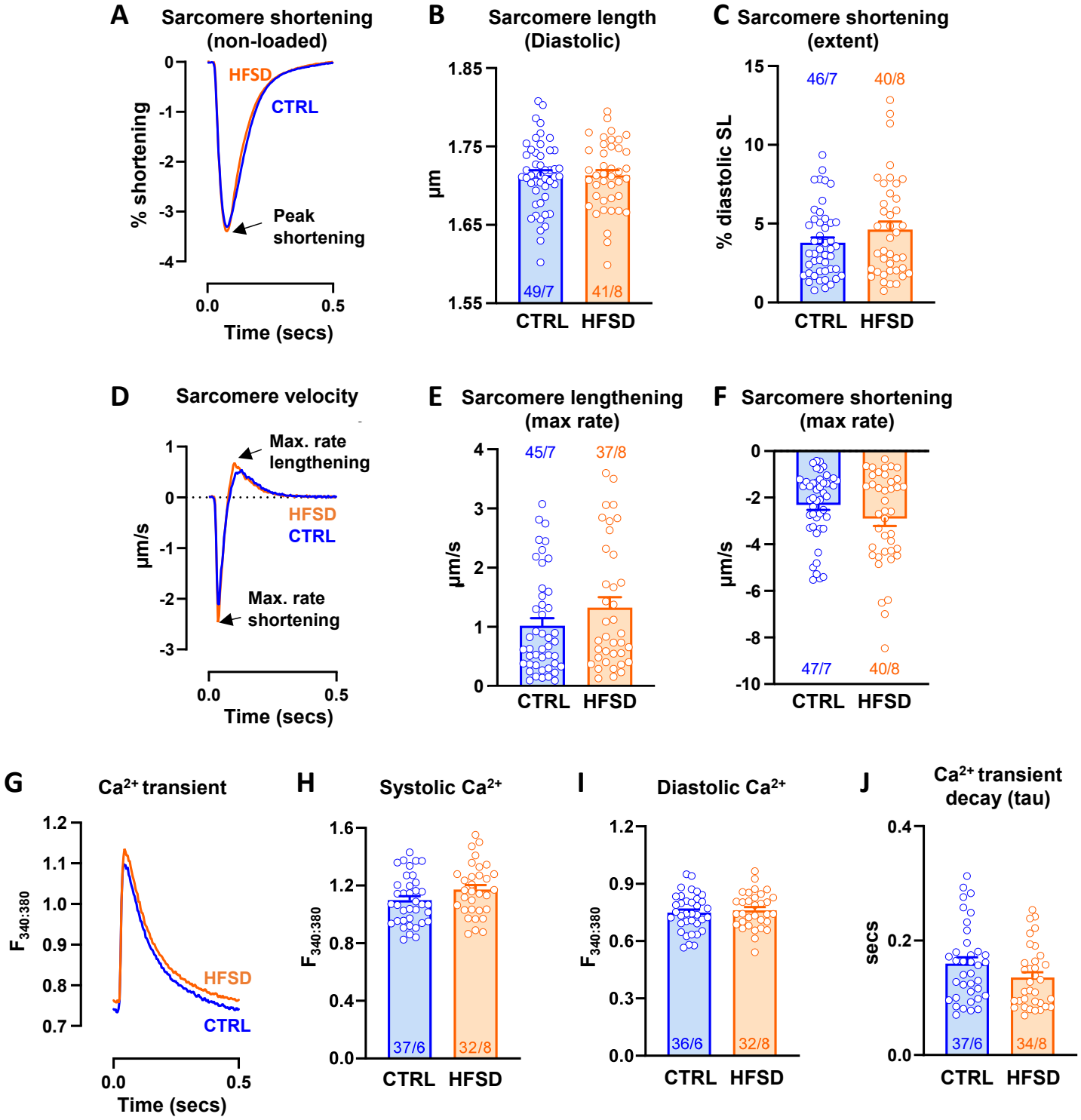
A
Sarcomere shortening (non-loaded)
% shortening
HFSD
CTRL
Peak shortening
Time (secs)
B
Sarcomere length (Diastolic)
µm
49/7
41/8
CTRL HFSD
C
Sarcomere shortening (extent)
% diastolic SL
46/7
40/8
CTRL HFSD
D
Sarcomere velocity
µm/s
Max. rate lengthening
HFSD
CTRL
Max. rate shortening
Time (secs)
E
Sarcomere lengthening (max rate)
µm/s
45/7
37/8
CTRL HFSD
F
Sarcomere shortening (max rate)
µm/s
47/7
40/8
CTRL HFSD
G
Ca2+ transient
F340:380
HFSD
CTRL
Time (secs)
H
Systolic Ca2+
F340:380
37/6
32/8
CTRL HFSD
I
Diastolic Ca2+
F340:380
36/6
32/8
CTRL HFSD
J
Ca2+ transient decay (tau)
secs
37/6
34/8
CTRL HFSD

Fig.2 Non-loaded sarcomere and Ca^{2+} dynamics in CTRL and HFSD cardiomyocytes.
A. Mean sarcomere contraction cycles presented as a percentage of diastolic sarcomere length for CTRL and HFSD cardiomyocytes
B-C. Mean diastolic sarcomere length and extent of sarcomere shortening for CTRL and HFSD cardiomyocytes.
D. Mean sarcomere shortening and lengthening rate records (time derivative of sarcomere contraction-relaxation cycle) for CTRL and HFSD cardiomyocytes. The nadir and zenith represent maximal shortening and lengthening rates respectively.
E-F. Maximal rate of lengthening and shortening rates for CTRL and HFSD cardiomyocytes.
G. Mean Ca^{2+} transient records for CTRL and HFSD cardiomyocytes.
H-J. Mean Ca^{2+} levels (systolic and diastolic) and time constant of transient decay (*tau*) in HFSD and CTRL cardiomyocytes.

Mean data computed from average of 20 cycles per cardiomyocyte to derive group mean (N = 6-8 mice per group, n = 32-49 cells per group). Comparisons between two treatment groups performed using student's t-test (all $p>0.05$, ns). Data presented as mean $\pm$ standard error of the mean.

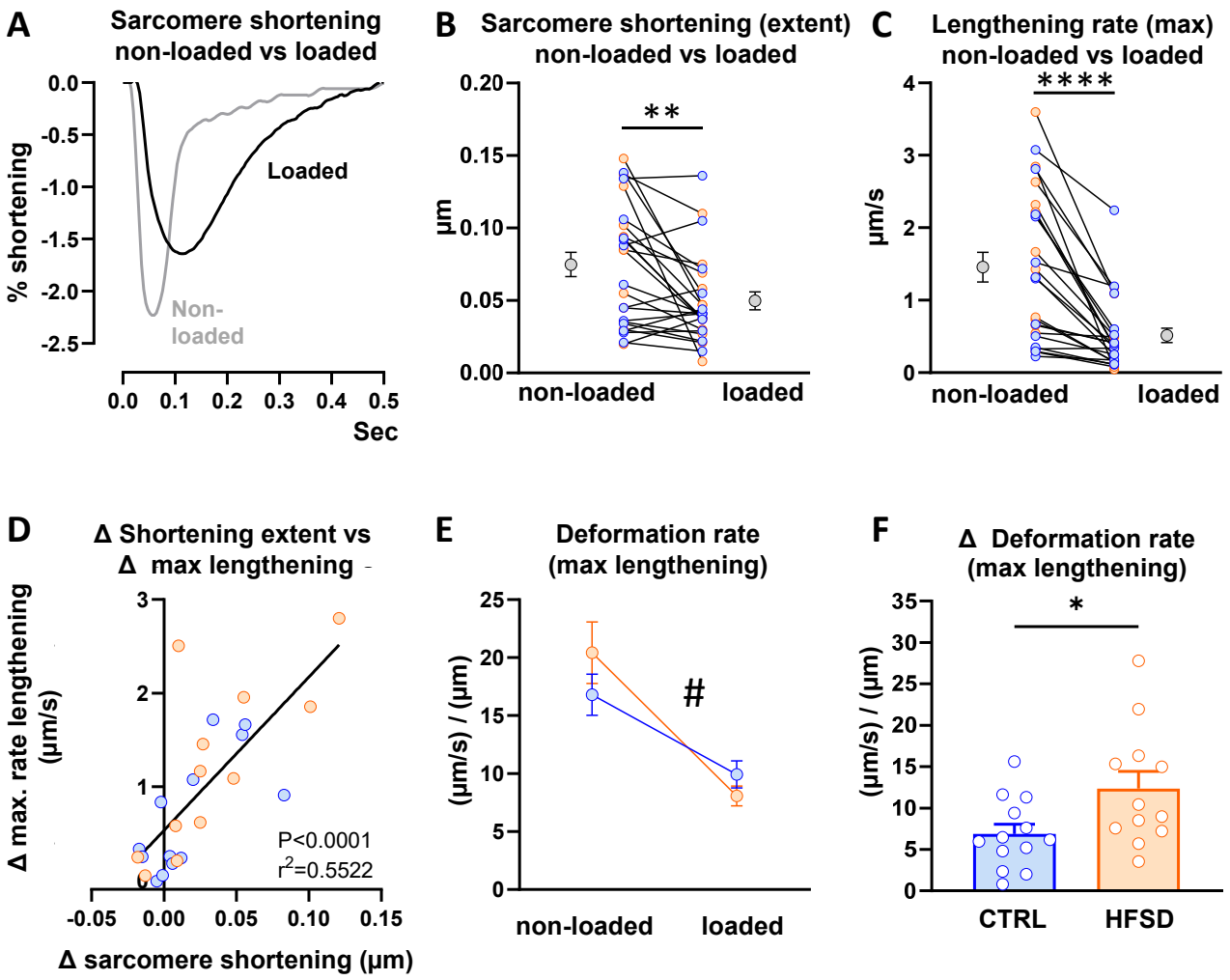

Fig. 3 Sarcomere shortening and lengthening in non-loaded and loaded pacing states.
A. Exemplar non-loaded and loaded sarcomere contraction cycles for the same cardiomyocyte (CTRL).
B-C. Extent of sarcomere shortening and maximum rate of lengthening, measured for each cardiomyocyte in non-loaded and loaded state for CTRL and HFSD groups combined (N = 9 mice, n = 25 cells). Mean data for CTRL and HFSD are presented as grey points to the left (non-loaded) and right (loaded) of individual cardiomyocyte data.
D. Correlation of loading associated sarcomere shortening change and maximum rate of lengthening change for CTRL and HFSD combined.
E. Mean loading effect on maximum deformation rate during lengthening ((µm/s) / (µm); maximum rate of lengthening (µm/s) normalized by shortening extent (µm)) for CTRL vs HFSD. (CTRL: N = 5 mice, n = 13 cells; HFSD: N = 4 mice, n = 12 cells). Significant ANOVA interaction effect (diet treatment x load state).
F. Mean decrement in deformation rate during lengthening ((µm/s) / (µm)).

Comparison of cardiomyocyte responses in different loading conditions analysed by paired t-test. Comparison of cardiomyocytes from different treatment groups analysed by unpaired t-test. A 2-way ANOVA with repeated measures used for analysis of two independent variables. Data fitted with linear regression model and calculation of Pearson's correlation coefficient. Data presented as mean ± standard error of the mean. *p<0.05, **p<0.01, ****p<0.0001, #p<0.05 ANOVA factor interaction.

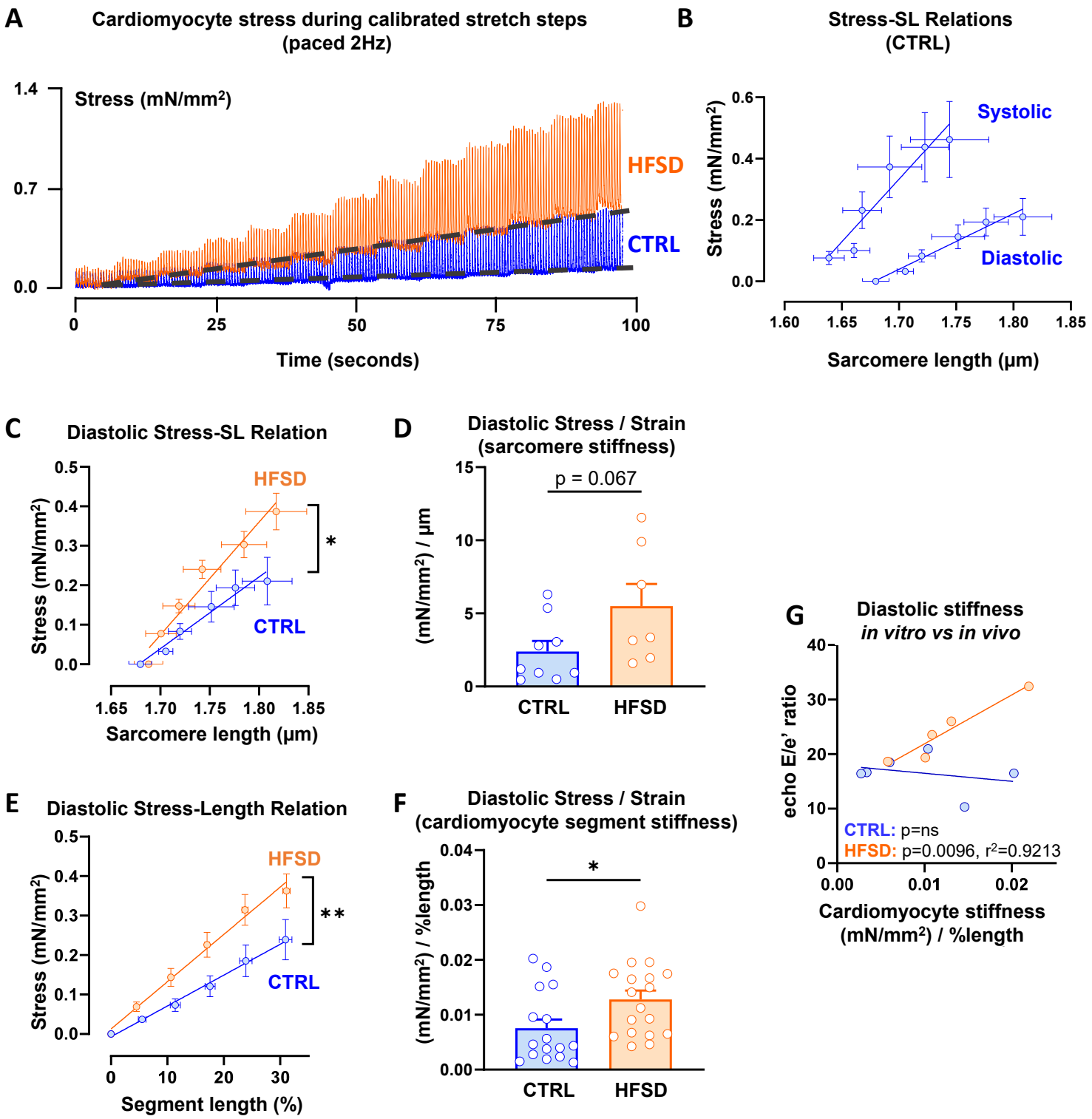
A
Cardiomyocyte stress during calibrated stretch steps
(paced 2Hz)
Stress (mN/mm²)
1.4
0.7
0.0
HFSD
CTRL
0
25
50
75
100
Time (seconds)
B
Stress-SL Relations
(CTRL)
Stress (mN/mm²)
0.6
0.4
0.2
0.0
Systolic
Diastolic
1.60
1.65
1.70
1.75
1.80
1.85
Sarcomere length (µm)
C
Diastolic Stress-SL Relation
Stress (mN/mm²)
0.5
0.4
0.3
0.2
0.1
0.0
HFSD
CTRL
*
1.65
1.70
1.75
1.80
1.85
Sarcomere length (µm)
D
Diastolic Stress / Strain
(sarcomere stiffness)
(mN/mm²) / µm
15
10
5
0
p = 0.067
CTRL
HFSD
G
Diastolic stiffness
in vitro vs in vivo
echo E/e' ratio
40
30
20
10
0
CTRL: p=ns
HFSD: p=0.0096, r²=0.9213
0.00
0.01
0.02
Cardiomyocyte stiffness
(mN/mm²) / %length
E
Diastolic Stress-Length Relation
Stress (mN/mm²)
0.5
0.4
0.3
0.2
0.1
0.0
HFSD
CTRL
**
0
10
20
30
Segment length (%)
F
Diastolic Stress / Strain
(cardiomyocyte segment stiffness)
(mN/mm²) / %length
0.04
0.03
0.02
0.01
0.00
*
CTRL
HFSD

Fig. 4 Quantifying diastolic stiffness in CTRL vs HFSD cardiomyocytes using strain normalization methods
A. Exemplar stress recordings of CTRL and HFSD cardiomyocytes undergoing 'stress-length' protocol (2Hz paced). Diastolic baseline stress shifts indicated by broken line.
B. Diastolic and systolic sarcomere mean stress- sarcomere length (SL) relations in CTRL cardiomyocytes (N = 5 mice, n = 9 cells).
C. Diastolic mean stress-sarcomere length relation (linear regression fit) for HFSD and CTRL.
D. Diastolic stress (mN/mm^2) normalized relative to sarcomere stretch (µm) yields sarcomere stress/strain = stiffness [(mN/mm^2) /strain (µm)] for HFSD and CTRL.
E. Diastolic mean cardiomyocyte segment stress-length relation (linear regression fit) for HFSD and CTRL..
F. Diastolic stress (mN/mm^2) normalized relative to segment stretch (% length) yields cardiomyocyte segment stress/strain = stiffness [(mN/mm^2) /strain (% length)] for HFSD & CTRL.
G. Correlation (linear regression fit) of *in vitro* cardiomyocyte segment diastolic stiffness (stress/strain) with *in vivo* diastolic dysfunction E/e' (blood flow/wall motion) in CTRL and HFSD. Cardiomyocyte data averaged per heart.

Comparisons between two groups performed using student's t-test (*$p<0.05$, **$p<0.01$). Data fitted with linear regression model and calculation of Pearson's correlation coefficient, presented as mean ± standard error of the mean. For **A. & B.** (CTRL: N=5 mice, n=9 cells; HFSD: N=2 mice, n=7 cells). For **C.&D.** (CTRL: N=6 mice, n = 16 cells; HFSD: N=6 mice, n=18 cells).

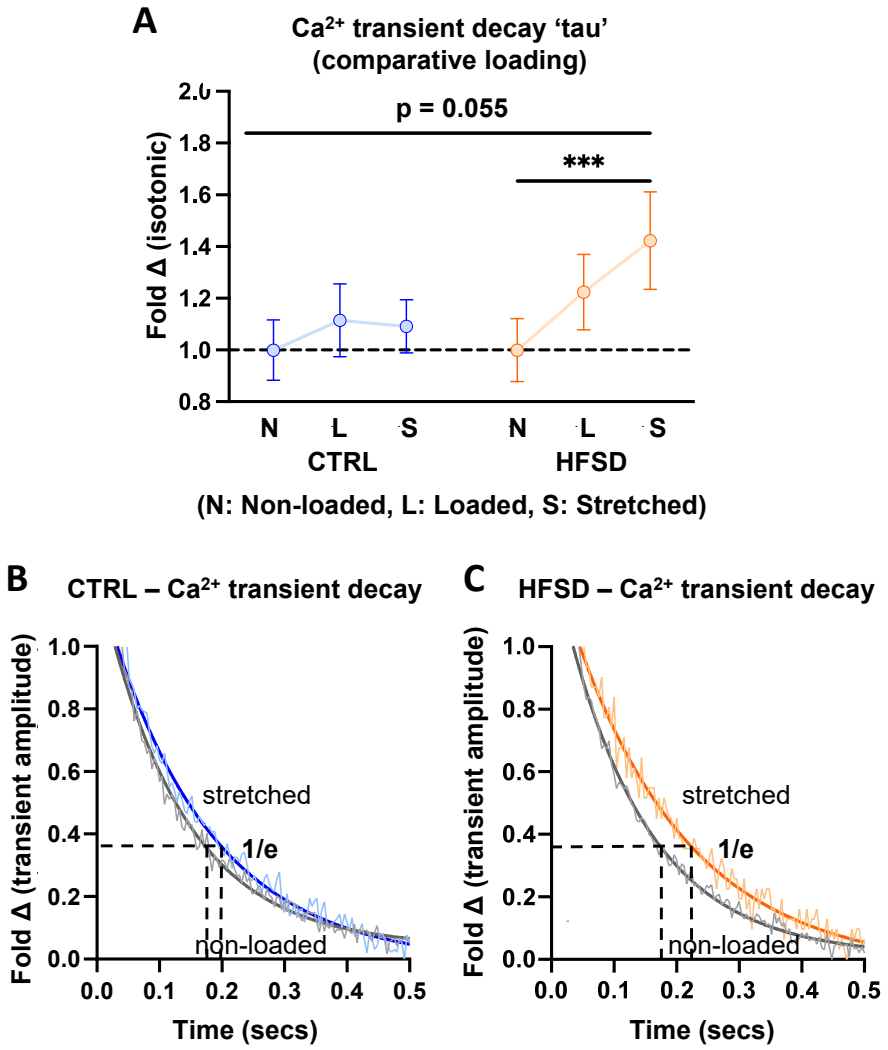

Fig. 5 Load dependence of cardiomyocyte Ca^{2+} transient decay in CTRL and HFSD cardiomyocytes.

A. Time constant of Ca^{2+} transient decay (tau) in cardiomyocytes with different load conditions: loaded (L) & stretched (S) shown as fold change relative to non-loaded (N) for CTRL and HFSD.
B-C. Exemplar Ca^{2+} transient decay records, with a mono-exponential decay function fit, in non-loaded and stretched CTRL and HFSD cardiomyocytes. Horizontal black broken lines intersect with mono-exponential fit at 36.8% (1/e) transient amplitude. Vertical broken lines from intersection points indicate the time constant of Ca^{2+} transient decay (tau).

For analysis of two independent variables a 2-way ANOVA with repeated measures used (CTRL: N = 5 mice, n = 13 cells; HFSD: N = 4 mice, n = 12 cells). Data are presented as mean ± standard error of the mean. ***$p<0.001$ (HFSD stretched vs non-loaded). Non-significant ANOVA interaction effect ($p = 0.055$, diet treatment x load state).

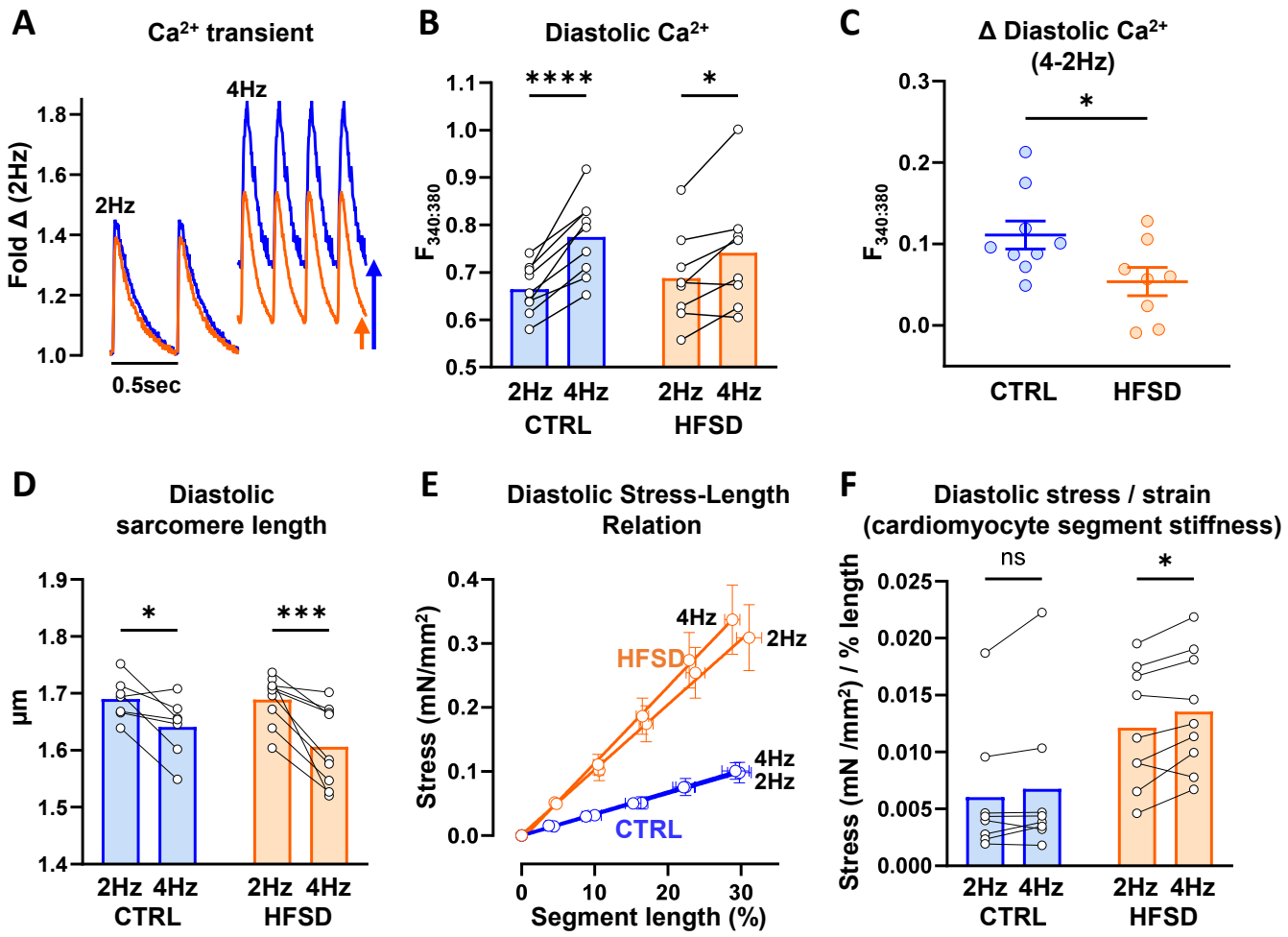

Fig. 6 Pacing induced changes in cardiomyocyte cytosolic Ca^{2+} levels and stiffness in CTRL & HFSD.
A. Exemplar CTRL and HFSD cardiomyocyte Ca^{2+} transients at 2 and 4 Hz pacing.
B. Diastolic cardiomyocyte Ca^{2+} levels measured before and after transition from 2 to 4 Hz pacing in HFSD & CTRL.
C. Diastolic cardiomyocyte Ca^{2+} level mean shift with transition from 2 to 4 Hz pacing in HFSD & CTRL.
D. Diastolic sarcomere length measured before and after transition from 2 to 4 Hz pacing in HFSD & CTRL.
E. Diastolic mean cardiomyocyte segment stress-length relation (linear regression fit) for HFSD and CTRL at 2 and 4 Hz pacing.
F. Diastolic mean cardiomyocyte segment stress-length relation slope (mN/mm^2) normalized relative to segment stretch (% length) yields cardiomyocyte mean segment stress/strain = stiffness [(mN/mm^2) /strain (% length)] for HFSD and CTRL at 2 and 4 Hz pacing.

Comparison between two groups performed using unpaired t-test. With two independent variables a repeated measures 2-way ANOVA Sidaks post-hoc analysis was performed (*$p<0.05$, **$p<0.01$, ****$p<0.0001$). Data are presented as mean ± standard error of the mean or mean with paired individual points. For **B. & C.** (CTRL: N = 4 mice, n = 9 cells; HFSD: N = 4 mice, n = 8 cells). For **D. & E.** (CTRL: N = 4 mice, n = 7 cells; HFSD: N = 4 mice, n = 9 cells). For **F.** (CTRL: N = 4 mice, n = 8 cells; HFSD: N = 4 mice, n = 9 cells).